KfK 3358
Mai 1982

Oxidation of Zircaloy 4 Tubing in Steam at 1350 to 1600°C

Atef E. Aly
Institut für Material- und Festkörperforschung
Projekt Nukleare Sicherheit

Kernforschungszentrum Karlsruhe

KERNFORSCHUNGSZENTRUM KARLSRUHE
Institut für Material- und Festkörperforschung
Projekt Nukleare Sicherheit

KfK 3358

Oxidation of Zircaloy 4 Tubing in Steam at 1350 to 1600 °C

Atef E. Aly

Kernforschungszentrum Karlsruhe GmbH, Karlsruhe

Kernforschungszentrum Karlsruhe GmbH
ISSN 0303-4003

Oxidation of Zircaloy 4 Tubing in Steam at 1350 to 1600 °C

A b s t r a c t

The oxidation behaviour of Zircaloy 4 (KWU-type) tubing in steam was investigated under Light Water Reactors (LWR) severe core damage conditions. Reaction kinetics were measured over the temperature range 1350 - 1600 °C.

The reaction kinetics were described by a parabolic rate of mass increase and ZrO_2 scale growth. The ZrO_2 scale preserved its protective nature up to the complete metal consumption. A discontinuity was found in the temperature dependence of the reaction rates of mass increase which is attributed to the change in the oxide microstructure at the discontinuity temperature (1550 °C). The results also indicated the severe degree of embrittlement induced by oxidation. The dependence of microhardness on dissolved oxygen concentration in the underlying metal has been established.

Oxidation von Zircaloy 4-Rohrmaterial in Dampf bei 1350 - 1600 °C

Z u s a m m e n f a s s u n g

Das Oxidationsverhalten von KWU-typischem Zircaloy 4-Rohrmaterial in Dampf wurde unter den Bedingungen eines schweren LWR-Coreschadens untersucht. Dazu wurden reaktionskinetische Messungen im Temperaturbereich von 1350 bis 1600 °C durchgeführt.

Die Reaktionskinetik kann durch einen parabolischen Verlauf von Massenzunahme und ZrO_2-Schichtdickenwachstum beschrieben werden. Die ZrO_2-Schicht behält ihre schützenden Eigenschaften bis zum totalen Konsum der metallischen Wandung. Ein diskontinuierlicher Verlauf der parabolischen Geschwindigkeitskonstanten als Funktion der temperatur bei etwa 1550 °C ist einer Transformation des oxidischen Kristallgitters von tetragonaler zu kubischer Struktur zuzuordnen. Die Ergebnisse erweisen gleichermaßen die mit der Oxidation einhergehende hochgradige Versprödung des Materials. Hierzu wird eine Beziehung zwischen Mikrohärte und Konzentration des gelösten Sauerstoffs vorgeschlagen.

Content

1. Introduction

The high temperature Zircaloy-steam oxidation has received wide attention due to the important role oxidation plays in contributing to the sources of heat that would have to be removed by the emergency core cooling systems (ECCS) in the event of an accident and also due to the oxidation induced embrittlement.

Oxidation of Zircaloy in steam at temperatures above the $(\alpha + \beta)/\beta$ transformation temperature generally results in two distinct product layers growing into the host beta, a superficial layer of ZrO_2 and an intermediate layer of oxygen-stabilized-α. During cooling to room temperature, the beta core transforms back to alpha with a significant different appearance than the stabilized-α. Within these temperatures it is generally accepted that the rate determining step of Zircaloy-steam reaction is the diffusion of oxygen anions via an oxygen deficient form of ZrO_2 where the parabolic law describes the kinetics /1/.

The limited data available for the high temperature reaction kinetics of Zry and steam and the experimental difficulties associated with accurately measuring the reaction rates were the main reasons for proposing the highly conservative model of Baker-Just /2/ for use in licensing calculations. This gave rise to the need for intensive research work to be carried out by several projects, that specifically address the kinetics of the Zry-steam reaction, with the aim of quantifying the degree of canservatism of Baker-Just correlation.

Ocken /3/ reviewed the recent measurements of Zry-steam oxidation reaction kinetics for the purpose of evaluating an improved model to replace that of Baker-Just. The author reported that the kinetics measurements fall into two groups according to the speciment heating method (Table 1). The externally heated specimen data show the larger activation energy and preexponential term. This effect of the heating method

was atributed to the presence of different temperature gradients across the oxidized layers. With externally heated specimens, the temperature of the oxide will be higher than that of the underlying metal, with the converse for the internally heated specimens /3/. It was reported that the measured oxide / stabilized-α thickness ratios are in general agreement with this thermal gradient effect /4/. Ocken /3/ in his recent review came to a conclusion that the parabolic reaction rate constant derived from the experiments that used internal heating of the specimens would be conservative for use in licensing calculations and the best-estimate fit to the data yielded A = 2 x 10" (mg Zr/dm^2)/min. and B = 33.6 Kcal/mole for the constants in the equation Kp = A exp (-B/RT).

Oxidation kinetics studies with Zircaloy tubing at temperatures related to severe core damage conditions (1300 ^{o}C < T<2000č) are limited and not familiar. Above the cubic-tetragonal phase transformation temperature for ZrO_2 (1577 ^{o}C), the oxidation kinetics change, as first suggested by Klepfer /5/. Urbanic and Heidrik /6/ reported not only a change in the reaction activation energy, as suggested by Klepfer, but also a discontinuity in the Arrhenius plot. Higher pre-exponential factor and higher activation energy for the oxidation reaction was a consequence of this phase transformation. Another change in the activation energy of the Zr-oxygen oxidation reaction was observed by Pemsler /7/ at 890 ^{o}C, which was attributed to the monoclinic-tetragonal allotropic transformation of ZrO_2.

This report presents the results of Zry-4 tubings oxidized in flowing steam under isothermal conditions at 1350 to 1600 ^{o}C. The significant parameters are compared to the previously obtained data.

2. Experimental

2.1 Material

The Zry-4 test tubings were 30 mm long tube sections in PWR typical dimensions (10.75 mm outer dia and 0.725 mm wall thickness). Prior to oxidation, the tubings were pickled in a mixture of nitric and hydrofluoric acids for 2 min and then rinsed in distilled water.

2.2 Experimental Techniques

2.2.1 Kinetics Measurements

Oxidation experiments were carried out in a closed, non-pressurized loop (fig 1) consisting of a tubular furnace with alumina reaction tube, steam condensers, by-pass condenser, temperature recorder and an argon flooding system. Temperature control was performed by a Pt/Pt-18% Rh thermocouple. The thermocouple was spot welded with an Ir-tab to the Zry tubing. Before running the experiment the specimen was kept in an argon flow of best commercial quality for about two hours. Mass increase measurements were carried out using analytical balance (type, Sartorius-2004 MP6) with accuracy of $\pm$ 1 x 10^{-5}g.

2.2.2 Microhardness Measurements

The microhardness across the tube wall of some oxidized test samples was measured using a microhardness tester (Type Reichert) with load of 25 g.

2.2.3 Morphology and Structure

Metallography covered all aspects of polished and etched cross-sections in order to reveal both the oxide and the structure of the underlying metal and measure the layer thicknesses. Fractography of the oxidized was also carried out using a SEM (model ISI-100).

2.3 Test Performance

During test performance, three main experimental problems came up. These problems were concerned with the steam condensing system, the alumina reaction tube and the exothermic

reaction between Zry and steam.

Due to the inefficient condensing system used initially, which was of small size, the steam pressure inside the boiler was gradually increasing causing flowing of water out of the boiler. By changing the condensing system, which improved the condensing efficiency, the above mentioned problem was overcome.

During the preliminary experiments two reaction tubes failed by cracking. After careful investigation, it was found that the cause of those cracks was the condensation of steam at the inlet-side above the reaction tube. In order to overcome this problem, the upper flange cooling system was cancelled and also a tape heater was used to superheat the steam lead pipe.

The most serious difficulty which had to be tackled was the sharp and fast temperature increase of the specimen, due to the exothermic reaction between Zry and steam followed by a slower decrease due to the diminishing reaction rate. This reaction can be described by the following equation:

$Zr + 2H_2O \rightarrow ZrO_2 + 2H_2 + \Delta H$ (heat) ... (ΔH = 210 KCal/mole at 1300K)

The increase in temperature due to this exothermic reaction eg. at 1100 ^{o}C is about 190 ^{o}C, at 1200 - 1300 ^{o}C about 240 ^{o}C and at 1500 ^{o}C the temperature increase is about 500 ^{o}C. Thus specimen positioning in the reaction tube in the argon flow before admitting steam is so important in overcoming this sharp temperature increase and its damaging effect.

The First Trial was putting the specimen in the constant temperature zone in the argon flow, then admitting steam, and when the steam reached the specimen and the exothermic reaction started (indicated by the sharp temperature increase of the specimen) the specimen was pulled down to a lower position to compensate for this increase in temperature and then moving the specimen up to the constant temperature zone (C.T.Z.). The result of this trial was negative. In the Second Trial the specimen was put in the argon flow at a position corresponding to a temperature of

1100 °C. Admitting steam caused an increase in temperature, as mentioned before, to reach a value of about 1300 °C (which is lower than the lowest temperature in this study). When the effect of the exothermic reaction diminished the specimen was pushed to C.T.Z. The results of this trial were also negative due to the uncontrolled sharp temperature increase of specimen.

The Third Trial was, keeping the specimen at the lowest position in the reaction tube (zero position) in the argon flow. The steam was admitted and the specimen raised gradually to C.T.Z. in about 60 seconds. The results of this trial were absolutely positive and it was possible to control the increase in the specimen temperature as a result of the exothermic reaction.

Inspite of the importance of the above mentioned sharp heating effect of the exothermic reaction between Zry and steam (T > 1300 °C), which disturbs the kinetic results, some projects /5,6/ that specifically address the kinetics of the Zry-steam reaction at these high temperatures (T > 1300 °C) did not explain how they control and avoid this specimen selfheating due to the exothermic reaction. From the above mentioned trials carried out in order to control this sharp and high temperature increase of the specimen, at the moment the steam reaches the Zry tubing, we can come to a conclusion that it is so difficult rather impossible to avoid this selfheating and the sharp temperature increase of the specimen without forming pre-oxide film preventing this specimen selfheating. Heating the specimen transiently in steam to reach the reaction temperature protected with an oxide film, formed during this transient specimen heating period, satisfactory prevented this selfheating effect of the exothermic reaction.

3. Results

3.1 Oxidation Kinetics

The kinetics data obtained are shown in table 2 and figures 2 and 3. The linear relationship between the square of the weigh gain (Δw^2) and oxidation time (t) indicates that, within this temperature range of investigation (1350 - 1600 °C), the Zry/steam

oxidation reaction obeys parabolic kinetics.

The parabolic rate constants, kp, were obtained from the slopes of the Δw^2-t plots (fig. 2). From the arrhenius plot of the temperature dependence of kp, a discontinuity was shown at temperature of $\sim$ 1550 ^{o}C. The activation energy of the Zry-4/steam oxidation reaction changed from $\sim$ 38 k.ca/mole at temperatures below the discontinuity temperature to a value of about 51 k.ca/mole at temperatures above this continuity temperature.

3.2 Oxidation-Induced Deformation

The stresses generated in the Zry tubings, due to oxidation, resulted in tubing strain in the radial as well as in the axial directions, ε_R and ε_A, respectively. The oxidation-induced radial strain is characterized by uniform and non-uniform strain periods (fig. 5). The amount of induced radial strain (ε_R) increases with both temperature and time (fig. 6). The results shown in fig. 7 and table 1 indicate that the oxidation-induced axial strain is always lower than the induced radial strain.

3.3 Microhardness

The microhardness measurements taken across oxidized tubings are shown in tables 3-8 and figures 8-11. A hardness gradient exists across the tube wall, with that material nearest to the metal-oxide interface being harder than that near the center of the tubing (fig. 12). The results given in figures 8-11 indicate that the microhardness number increases with both, temperature and time.

The oxygen concentration profiles across the tubing wall are given in figures 13 and 14. The values of the oxygen concentration were obtained from the microhardness numbers using the following relation /8/:

$c_\alpha = 1.4 \times 10^{-2} H_\alpha - 4.4$

$c_\beta = 3.1 \times 10^{-3} H_\beta - 0.39$

c = O_2-concentration (wt%)

H = Microhardness MHV 0.025 (kp/mm^2)

The above mentioned relation assumes, as a simplification, that the contribution to the hardness due to oxygen uptake, is proportional and additive and no influence of the state of preparation (temp. and time).

The results indicate that the oxygen concentration across the metallic phases, stabilized-α and transformed B-Zr, dropped to lower values in the material nearest to the mid-wall position (fig. 13).

3.4 Metallography and Fractography

The features of the oxidized Zry tubings are shown in figures 15-19. The outermost layer is ZrO_2. Adjacent to the oxide is a layer of α-Zr(O) overlying a transformed B-Zr matrix. The oxide film formed on all specimens was a double layer of columnar grains divided in two parts by an interface containing metallic (tin-rich) particles (figures 15-19). After metallography these two layers of the oxide were well defined by either the presence of a plane of voids or a complete separation of the two layers (fig. 20). For temperatures higher than 1500 °C, metallography (fig. 21) revealed an additional internal partial layer consisting of oxide grains and metallic (α-Zr(O)) stringers at grain boundaries. The relative thickness of this internal partial layer is higher for 1600 °C compared to 1550 °C (fig. 21). Figures 22 and 23 reveal the vanishing effect of prolonged time of oxidation on the volume fraction of (α-Zr(O)) stringers in the oxide.

Fracture surface investigation of the oxidized tubing reveals the severe brittle fracture of the tubing wall which is mostly of stabilized-α (fig. 24) and a separation line resulting from the formation of the tin-rich precipitates /6,9/.

4. Discussion

4.1 Oxidation Kinetics

The parabolic rate law describing the kinetics is usually taken as evidence that the rate determining step of the reaction is

a solid state diffusion process occuring within the oxide film barrier /10/. The oxide film formed on alloys of Zr is generally accepted to be an oxygen deficient form of ZrO_2 with the defect being oxygen-anion vacancies /9, 11/.

The results are in agreement with those of Urbanic and Heidrick /6/, who measured, using the hydrogen evolution method and weight gain method, the rates of the reaction between Zry-2 and -4 and steam in the temperature range 1050 - 1850 ^{o}C. White /12 - 14/ established parabolic rate constants for the reaction of Zry-2, Zry-4 and Zr-2.0 at.% Cr - 0.16% Fe (Valoy) with steam in the temperature range 1200 - 1810 ^{o}C. With inductively heated Zry-4 tubings in steam in the temperature range 1300 - 1450 ^{o}C, Leistikow et al. also indicated parabolic kinetics /15/. Cathcart and co-workers /16/ reported that parabolic rate law fit the isothermal oxidation kinetics results of isothermally oxidized Zry-4 in steam with the temperature range 900 - 1500 ^{o}C.

The discontinuity in the temperature dependence of Kp at temperature of 1550 ^{o}C (fig. 4) is a result of the change in the activation energy of the oxidation reaction. The activation energy of the reaction changed from about 38 Kcal/mole for the temperatures lower than the discontinuity temperature to a value of about 51 k.cal/mole for the temperatures higher than that temperature. This observed change in the pre-exponential factor and the activation energy of the oxidation process can be attributed to the allotropic transformation of the ZrO_2 from tetragonal to cubic structure. Urbanic and Heidric /6/ also reported that there was a discontinuity in the temperature dependence of the reaction rate of Zry-4 with steam at temperature of 1580 ^{o}C and attributed this to the change in the oxide microstructure at the discontinuity temperature. So the result of the present work is judged to be reasonable. However, the difficulties in evaluating the kinetic results and the uncertainty in temperature measurements contribute to relativate

the discontinuity and the change in activation energy.

Table 9 lists the parabolic reaction rate constant, Kp for Zircaloy 4 specimens oxidized at different temperatures by different investigators.

The low values of the oxidation rate constants obtained from the present investigation is due to the effects of preoxidation on the subsequent oxidation. As a consequence of the test performance method used, where the specimen brought to the isothermal reaction temperature transiently, the oxide film formed during the heatup period inhibits the subsequent oxidation process.

The effect of preoxidation on Zry-steam oxidation kinetics has been studied by Biederman and co-workers /7/. In this investigation Zry-4 tubings in both as-received and pre-oxidized conditions have been oxidized in the temperatures 982, 1093, 1205 and 1316 ^{o}C. The authors reported that the pre-oxidized tubings oxidized slower than the as-received specimens. Moreover, for preoxidized specimens, both oxide and oxide + stabilized-α layer thicknesses vary linearly with the square root of time indicating that preoxidized Zry tubing obeys a parabolic oxidation law.

As reported by Ocken /2/ the high temperature Zry-steam oxidation data fall into two groups according to the methods used to heat the specimens. From the regression analysis of the data that considers the specimen heating method (table 1), we can come to a conclusion that the value for the activation energy determined from the present results (37.8 Kcal/mole) is in a good agreement with that of specimens externally heated (41.2 Kcal/mole) and in excellent agreement with that value obtained from the regression analysis of all measurements obtained from both heating methods; internal and external methods, (37.8 Kcal/mole).

4.2 Oxidation-Induced Deformation

Large compressive stresses are generated in the growing oxide film of Zr and its alloys /18/ due to the inward anionic mobility /19/ and the high Pilling-Bedwarth Ratio of ZrO_2 (1.44 for the monoclinic phase). These compressive stresses constrained in the oxide film may be relieved by plastic deformation of the oxide film /20/, and / or the metal substrate as well as fracture of the oxide /21, 22/.

The experimental results of this work, as well as the results obtained by oxidizing different types of Zircaloy tubings (Zry-4 and -2) in air atmosphere within the temperature range 650-1100 ^{o}C /23/, indicate that deformation of the underlying metal is a considerable mechanism of relieving the stresses generated during oxidation. The compressive stresses in the oxide film generate tensile hoop stresses as well as tensile stresses in the axial direction of the tube. If these tensile stresses exceeds the flow stress of the metal plastic deformation occurs. When the rare of stress generation becomes higher than that of stress relief by metal deformation, cracking of the oxide may contribute as an additional stress relieving mechanism.

4.3 Metallography

The protective nature (compactness and adherence) of the oxides formed at all investigation temperatures and up to the complete metal consumption (fig. 15 - 19) is consistent with the kinetics results indicating a parabolic behaviour.

The increased amount of α-Zr stringers in the oxide above the discontinuity temperature (fig. 21) is in agreement with the Zr-O phase diagram /24/. According to the Zr-O phase diagram, at temperatures higher than 1500 ^{o}C the B-Zr reacts with oxygen to form a layer of tetragonal ZrO_2, a layer of cubic ZrO_2 and a layer of oxagen stabilized α-Zr. Upon cooling through the first discontinuity temperature (1500 ^{o}C) the cubic ZrO_2 undergoes an eutectoid decomposition to form a tetragonal form

Of ZrO_2 and α-Zr of a volume fraction of about 10%. Another eutectoid decomposition occurs upon cooling through the second discontinuity temperature (< 1000 °C, according to Zr-O phase diagram). During this eutectoid decomposition the tetragonal ZrO_2 decomposed to a stable monoclinic ZrO_2 and α-Zr of about 1-2%.

The observed increase in the volume of α-Zr stringers (fig. 21) is an evidence of the allotropic transformation of ZrO_2 from tetragonal to cubic form with the resulting increase in the activation energy of the oxidation reaction process.

The observed microstructures (fig. 22 and 23) reveal the decreasing amount of α-Zr stringers in the oxide by prolonged time of oxidation. At 1600 °C the α-Zr stringers in the oxide were completely vanished after 5 minuntes oxidation time (fig. 23). Increasing the holding time at temperature, for the temperature above the discontinuity temperature, would result in saturation of the cubic ZrO_2 with oxygen to a hyper-eutectoid composition /24/. Upon cooling and depending on the holding time and the resulting degree of oxygen saturation, the cubic ZrO_2 would decompose to a tetragonal form of ZrO_2 and a decreased volume of α-Zr or it would transform to a total volume of tetrogonal ZrO_2. These results are in consistence with the Zr-O phase diagram (fig. 25).

4.4 Fractography and Microhardness

Fractography investigation showed the typical brittle fracture in the stabilized-α zone. The microhardness measurements revealed that the α-Zr being harder than that near the mid-wall position.

5. Conclusions

(1) Within the temperature range of investigation (1350 - 1600 °C), the parabolic rate kinetics describe the reaction rate as indicated by the kinetics plots and manifested by the protective nature of the oxides formed at all temperatures and up to the complete metal consumption.

(2) A discontinuity in the temperature dependence of the reaction rate is observed at 1550 ^{o}C which is attributed to the allotropic phase transformation of the oxide.

The increased amount of (α-Zr(O)) stringers in the oxide at and above the discontinuity temperature is an indication of the eutectoid transformation of the tetragonal oxide to cubic oxide.

(3) The severe embrittlement of the underlying metal, induced by oxidation, is indicated by the typical brittle fracture of the stabilized-α zone of the oxidized tubing.

(4) The microhardness measurements indicate the oxygen concentration profiles across the metallic phases, stabilized-α layer and transformed-B matrix.

(5) Compressive stresses generated in the oxide are compensated by tensile stresses in the underlying metal. Oxidation of the Zry tubing induces radial as well as axial strain. The radial strain is characterized by uniform and non-uniform periods.

6. Acknowledgements

The author[+] wishes to thank Eng.D.Jennert, Mr.H.v.Berg and Eng. R.Kraft for assistance during building the experimental set-up. Thanks also are due to Mrs.Bennek-Kammerichs for her help during the metallography work. The fruitful discussion with Dr.S.Leistikow and Mr.G.Schanz during finalizing the report is indebted. With profound gratitude, the author thanks the Institute of Material and Solid State Research (IMF-II) for giving the opportunity and extending the facilities to carry out this work.

[+] IAEA Guest Scientist, Dept. of Nuclear Metallurgy, Nuclear Research Center, Atomic Energy of Egypt

7. References

1. P.D.Parsons and W.N.Miller, ND-R-7(5)(1977)
2. L.Baker and L.C.Just, ANL-6548 (May 1962)
3. H.Ocken, Nuclear Technology 47 (1980) 343
4. H.Ocken, R.Biederman, C.Hann and R.Westerman, Proc. Fourth Int. Conf., Zirconium in Nuclear Industry, ASTM-STP-681, PP. 514-536
5. H.H.Klepfer, as reported by P.W.IANNI, "Metal-Water Reactions - Effects on Core Cooling and Containment" APED-5454, General Electric Co. (March 1968)
6. V.F.Urbanic and R.T.Heidric, J.Nucl. Mater. 75 (1978) 251
7. J.P.Pemsler, Electrochem. Technol. 4(3-4) (1966) 128
8. S.Leistikow, G.Schanz and H.v.Berg, KfK-2587 (Mar 1978)
9. G.J.Yurek, J.v.Cathcart and R.E.Pawel, Oxid Metals 10(1976) 255
10. K.Hauffe, "Oxidation of Metals", Plenum Press, N.Y. (1965)
11. B.Cox, "Advances in Corrosion Science and Technology", Ed.M. G.Fantana and R.W.Staehl, Plenum Press, N.Y, vol. 5, 1976, p. 173
12. J.F.White, GEMP-475 A, General Electric Co., Cincinnati, Ohio (1967)
13. J.F.White, GEMP-67, General Electric Co., Cincinnati, Ohio (1967)
14. J.F.White, GEMP-619, General Electric Co., Cincinnati, Ohio (1968)
15. S.Leistikow, H.v.Berg, R.Kraft and G.Schanz, 1980, unpublished work
16. J.v.Cathcart, R.E.Pawel, R.A.Mckee, R.E.Druschel, G.J.Yurek, J.J.Campbell and S.H.Jury, ORNL-NUREG-17(1977)
17. R.R.Biederman, R.D.Sission, J.K.Jones and W.G.Dobson, EPRI NP-734, Electric Power Research Institute (Mar 1978)
18. C.Roy and B.Burgess, Oxid Metals 2(1970)235
19. J.L.Whitton, J.Electrochem. 50c 115(1968) 58
20. L.H.Keys and P.Lacombe, J.Less, Common Metals 14(1968)181
21. D.H.Bradhurst and P.M.Heuer, J.Nucl.Mater. 37(1970)35
22. A.T.Donaldson and H.E.Evans, J.Nucl.Mater. 99(1981)38-57
23. F.H.Hammad. Atef E.Aly and S.M.El.Raghy, paper presented to the conference "Environmental Degradation of Engineering Materials", Sep 21-23, 1981, Virginia/USA
24. E.Gebhardt, H.D.Seghezzi and W.Dürrschnabel, J.Nucl.Mater. 4(1961)255

Table 1

Reaction Rate Constants for Zircaloy Oxidation According to Heating Arrangement /2/

Data Set	Number of Kp Values	Kp = Aexp -B/RT	
		$A(mgZr/dm^2)^2/min$	B(Kcal/mole)
Internal Heating	23	1.99×10^{11}	33.6
External Heating	34	2.48×10^{12}	41.2
All measurements	57	7.98×10^{11}	37.8
Baker-Just	5	1.99×10^{13}	45.5

Table 2

High Temperature Steam Oxidation of Zry-4 Tubings in the Range 1350-1600 ^{o}C

Temp. (^{o}C)	Time (min)	W.G. (mg/dm^2)	Measured Oxide (um)	Radial Strain (%)	Axial Strain (%)
1350	1	1237.89	-	1.4	1.33
	2	1446.68	-	1.86	1.50
	3	1666.68	-	1.87	1.67
	5	2061.26	90	2.34	1.83
	10	2803.84	130	3.72	1.83
	15	3526.21	160	4.19	2.00
	20	3897.63	-	7.91	3.17
	25	4152.58	200	6.54	2.67
	35	4934.32	-	14.02	4.15
	50	5916.00		-	-
	60	6389.32	-	-	-
1400	2	1927.32	-	-	-
	5	2559.84	100	2.34	1.83
	10	3618.00	-	3.26	2.33
	15	4338.11	180	8.84	3.66

Table 2
(continued)

Temp. (°C)	Time (min)	W.G. (mg/dm^2)	Measured Oxide (um)	Radial Strain (%)	Axial Strain (%)
	20	4850.42	-	7.48	3.17
	25	5332.16	260	13.55	3.83
	30	5266.53	-	-	-
	35	6059.26	-	17.21	3.49
	40	6638.26	-	-	-
1450	2	2514.47	-	2.34	1.50
	5	3144.05	110	3.26	1.83
	7	3487.74	-	3.27	2.00
	10	4043.42	170	3.74	2.16
	15	4666.79	240	4.67	-
	20	5252.26	-	-	-
	25	6038.21	340	-	-
	30	6392.53	-	-	-
	35	6450.89	-	-	-
	40	7000.63	-	-	-
1500	2	3189.21	-	2.80	1.67
	5	3674.74	150	3.74	1.83
	7	4004.74	-	4.65	2.33
	10	4713.58	230	4.19	2.50
	15	5397.58	340	4.19	2.50
	20	5980.53	-	6.05	3.17
	25	6546.89	380	7.44	3.00
	30	6877.47	-	10.23	3.66
1550	2	4590.53	220	4.57	2.33
	3	5133	-	4.65	2.50
	5	5553.37	270	5.12	3.00
	7	6319.42	-	6.07	3.00
	10	7040	380	7.44	3.67
	15	7383.58	440	11.16	4.49

Table 2
(continued)

Temp. (°C)	Time (min)	W.G. (mg/dm^2)	Measured Oxide (um)	Radial Strain+ (%)	Axial Strain+ (%)
1600	2	5638.26	330	4.65	2.50
	3	6420.05	350	5.58	3.00
	4	6815.26	-	6.05	3.16
	5	7191.95	470	6.98	4.33
	6	7302.21	-	10.23	5.83
	7	7466.26	-	10.70	5.67

$$\varepsilon_R = \frac{D_t - D_o}{D_o} \times 100 \qquad \varepsilon_A = \frac{L_t - L_o}{L_o} \times 100$$

Table 3

Microhardness Measurements
for Zry-4 Tubing Oxidized at 1350 °C for 1 min

Distance from Metal-Oxide (um)	SKt	HV	Distance from Metal-Oxide (um)	SKt	HV
20	45	869	320	61	469
40	47	762	340	61	469
50	50	673	360	58	503
60	47	762	380	57	525
80	52	637	400	57	525
110	56	548	420	55	560
120	57	525	440	67.5	395
140	61.5	450	460	61.5	450
160	61	454	470	50	673
170	60	390	480	72	327
180	63.5	421	500	52	645.5
200	74	311	520	61.5	450
220	79	274	530	49	707
240	77	287	540	53	599
260	72	327	560	48	743

Table 3
(continued)

Distance from Metal-Oxide (um)	SKt	HV	Distance from Metal-Oxide (um)	SKt	HV
290	62.5	438	580	45	847
300	70	345	600	42	974

Table 4

Microhardness Measurements
for Zry-4 Tubing Oxidized at 1350 ^{o}C for 2 min

Distance from Metal-Oxide (um)	SKt	HV	Distance from Metal-Oxide (um)	SKt	HV
10	41	1003	290	60	473
30	45	847	310	70	345
50	44	870	330	68	370
70	51	657	350	66	390
90	53	599	370	52	627
110	53	599	390	51	657
130	63	429	410	50	673
150	65	405	430	74	311
170	75	302	450	77.5	281
190	53	599	467	58	503
210	80	266	490	51	657
230	62	466	510	45	847
250	75	302	530	42	974
270	78	279	550	41	1003

Table 5

Microhardness Measurements
for Tubing Oxidized at 1350 °C for 3 min

Distance from Metal-Oxide (um)	SKt	HV	Distance from Metal-Oxide (um)	SKt	HV
15	40	1064	195	68	370
35	43	920	215	64	413
55	43	920	235	67	376
75	46	803	255	61	454
95	48	743	275	65	405
115	50	673	295	51	657
135	51	657	315	60	473
155	81	258	335	60	473
175	77	287			

Table 6

Microhardness Measurements
for Tubing Oxidized at 1400 °C for 5 min

Distance from Metal-Oxide (um)	SKt	HV	Distance from Metal-Oxide (um)	SKt	HV
30	45	847	280	55	560
50	45	847	330	58	503
80	46	803	380	53	599
130	50	673	430	48	743
150	49	707	450	46	803
180	52	627	480	45	847
230	54	585	500	45	847
250	49	707	520	41	1003

Table 7

Microhardness Measurements
for Tubing Oxidized at 1500 °C for 5 min

Distance from Metal-Oxide (um)	SKt	HV	Distance from Metal-Oxide (um)	SKt	HV
50	38	1168	290	49	707
110	42	974	340	42	762
130	43	920	390	50	673
180	43	920	410	48	743
230	43	920			

Table 8

Microhardness Measurements
for Tubing Oxidized at 1550 °C for 5 min

Distance from Metal-Oxide (um)	SKt	HV	Distance from Metal-Oxide (um)	SKt	HV
50	44	870	200	41	1003
100	45	847	220	44	870
150	41	1003			

Table 9

Zircaloy Oxidation Rates

Temperature °C	Kp, $(mg/dm^2)^2/min$		
	Present Study	Leistikow et al./8/+	Cathcart et al./16/
1350	0.67×10^6	0.773×10^6	0.909×10^6
1400	1.06×10^6	1.14×10^6	1.32×10^6
1450	1.27×10^6	1.64×10^6	1.87×10^6

+ From extrapolation of data obtained for the temperatures between 1000 and 1300 °C.

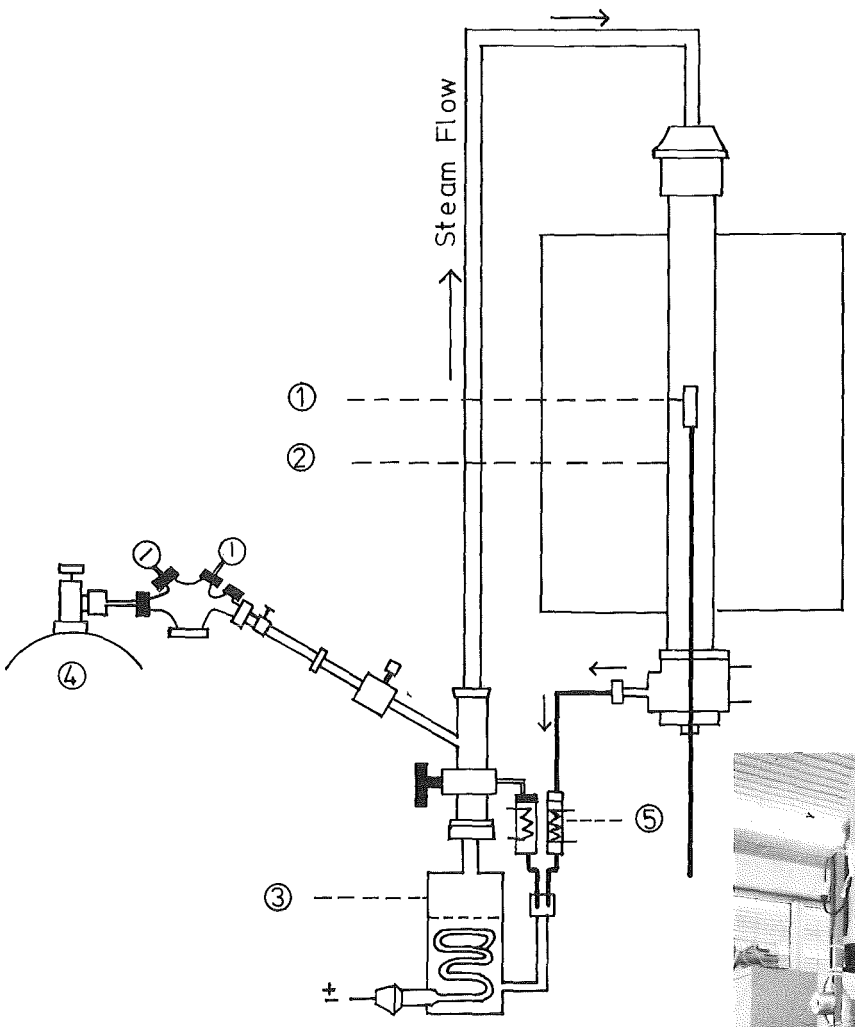

1. Zry-4 Tubing
2. Alumina Reaction Tube
3. Steam Generator
4. Argon Bottle
5. Steam Condensers

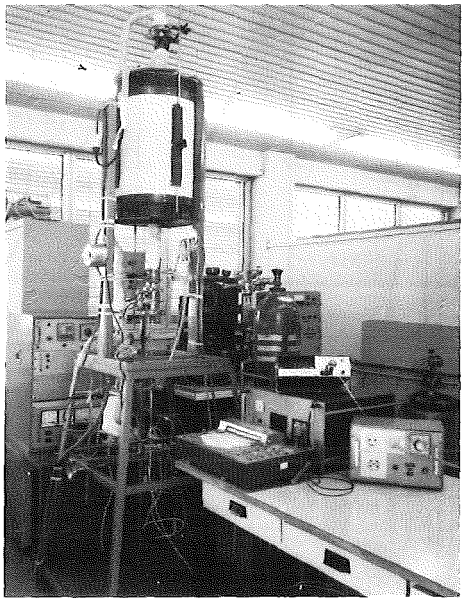

Fig. 1. High Temperature – Steam Oxidation Test Equipment

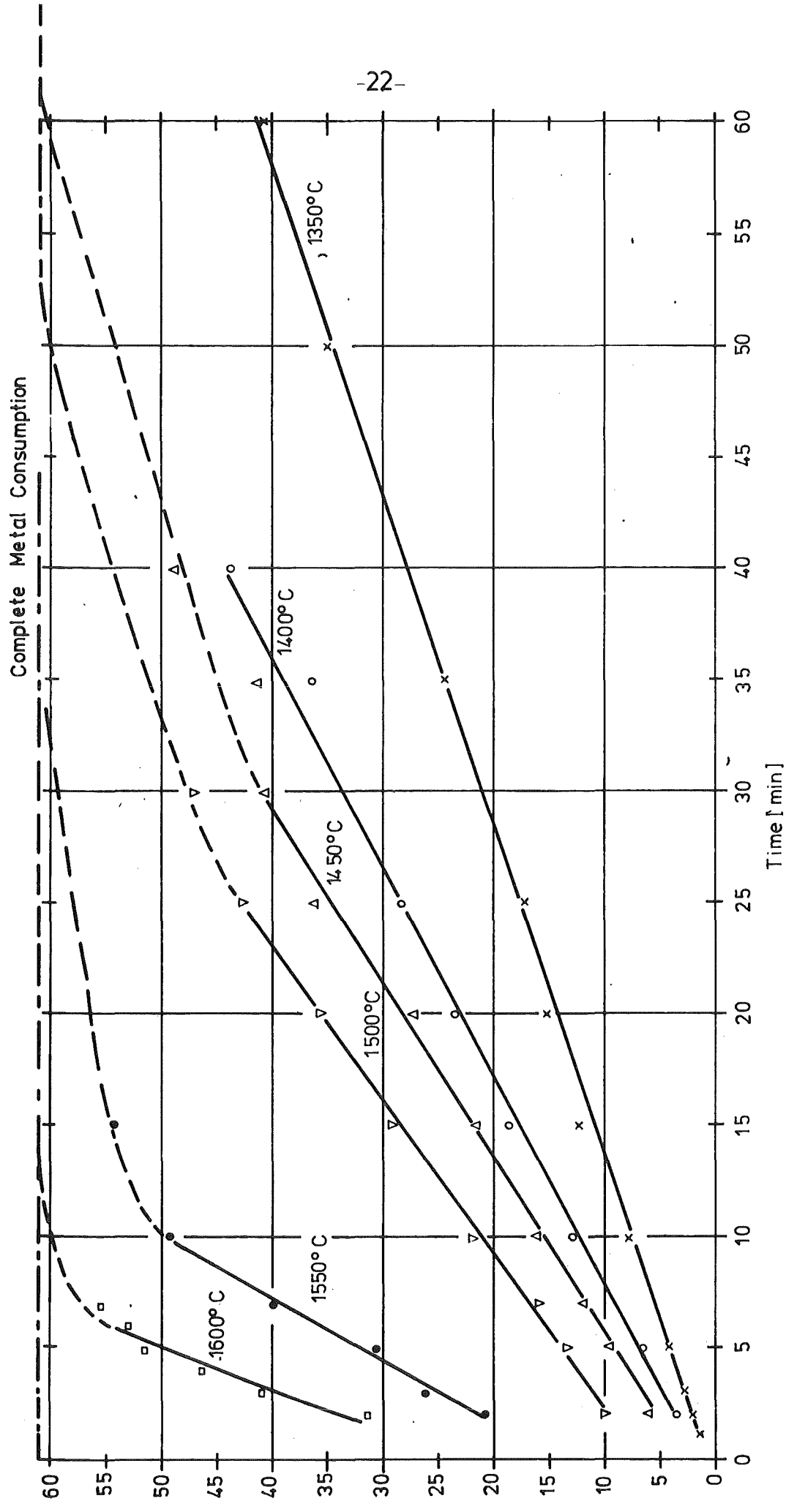

Fig.2 Parabolic Oxidation of Zry-4 Tubing

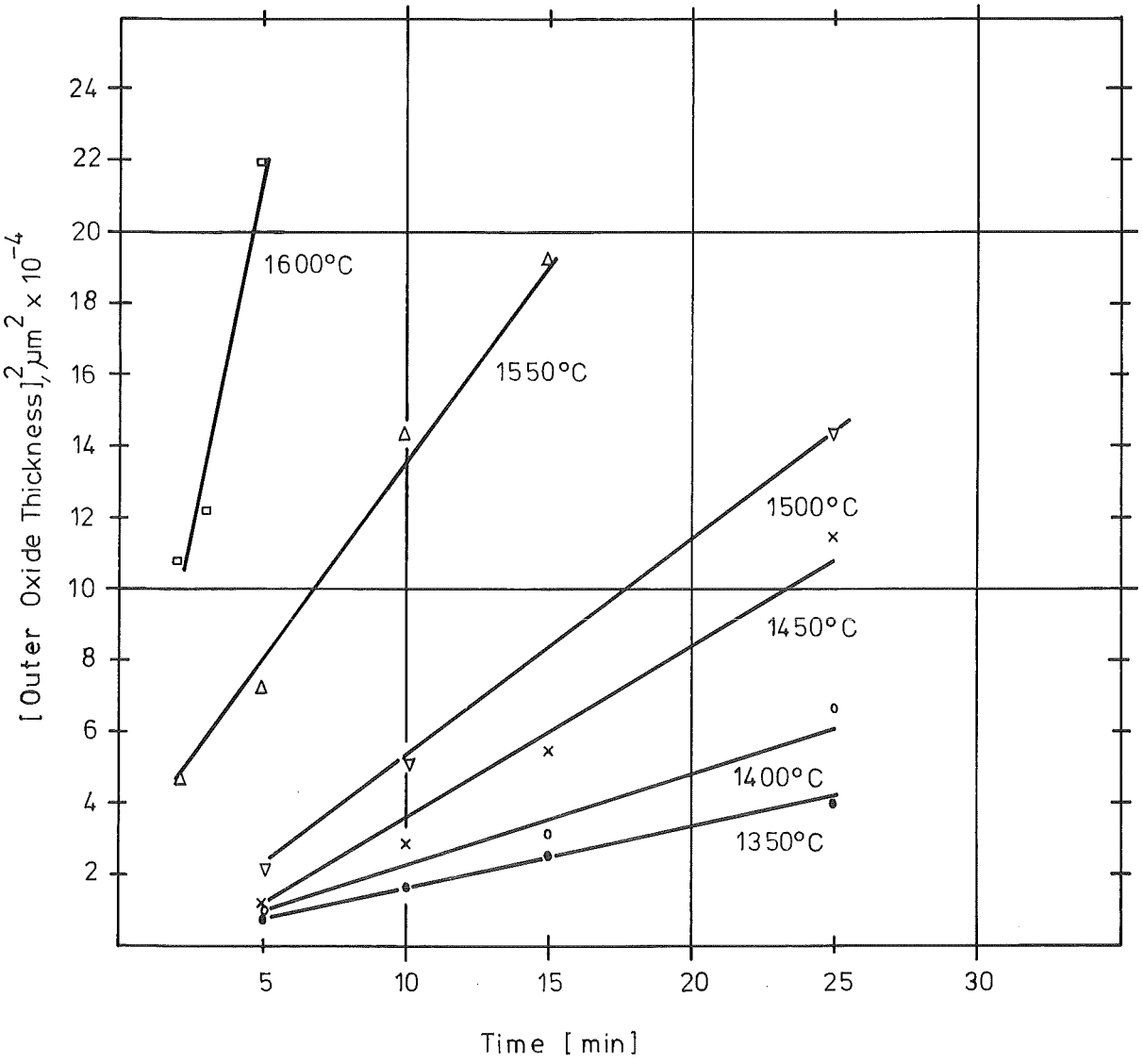

Fig. 3 Parabolic Growth of Measured ZrO_2 Layer Thickness

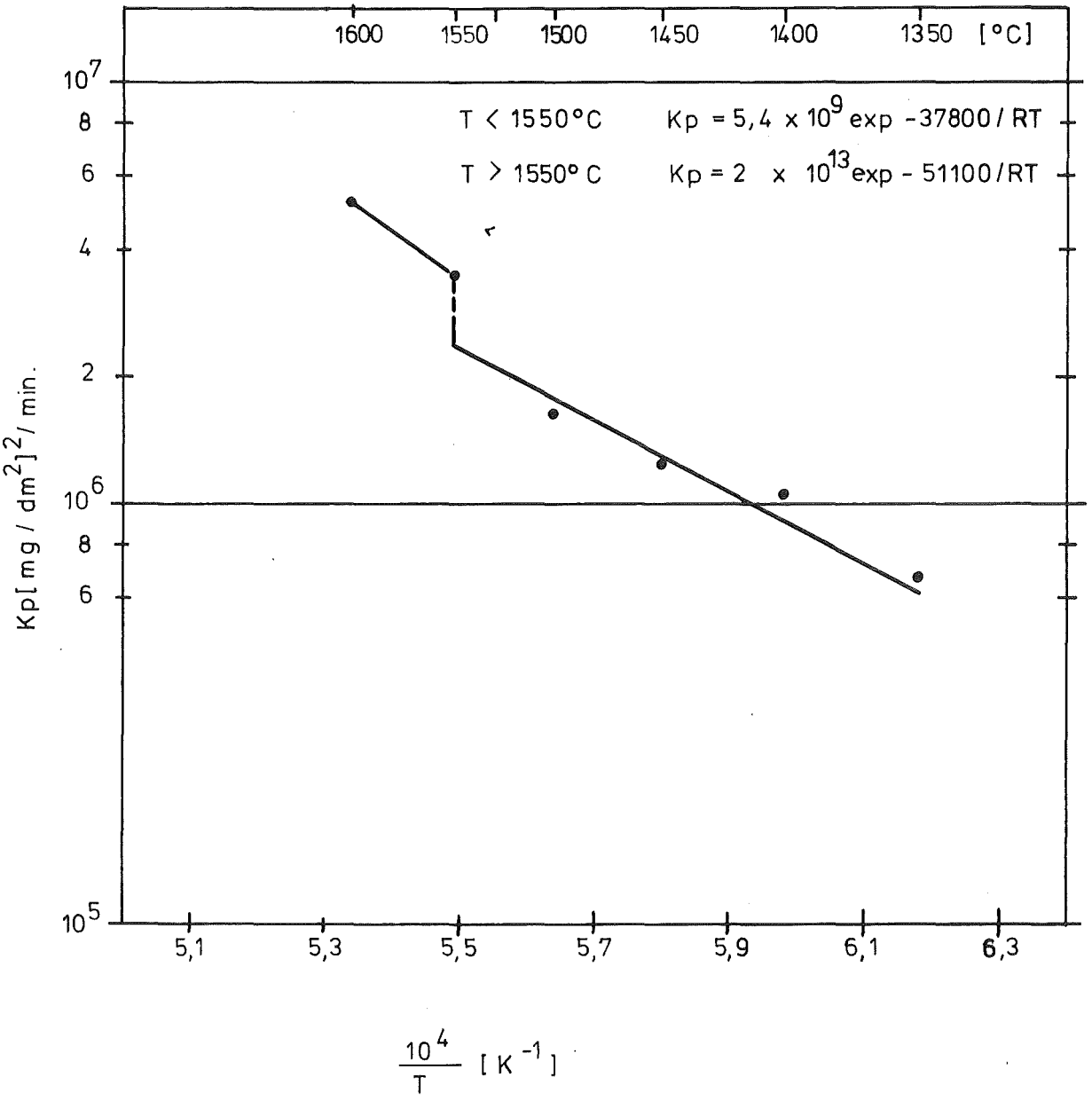

Fig. 4 Temperature Dependence of The Parabolic Oxidation Constant

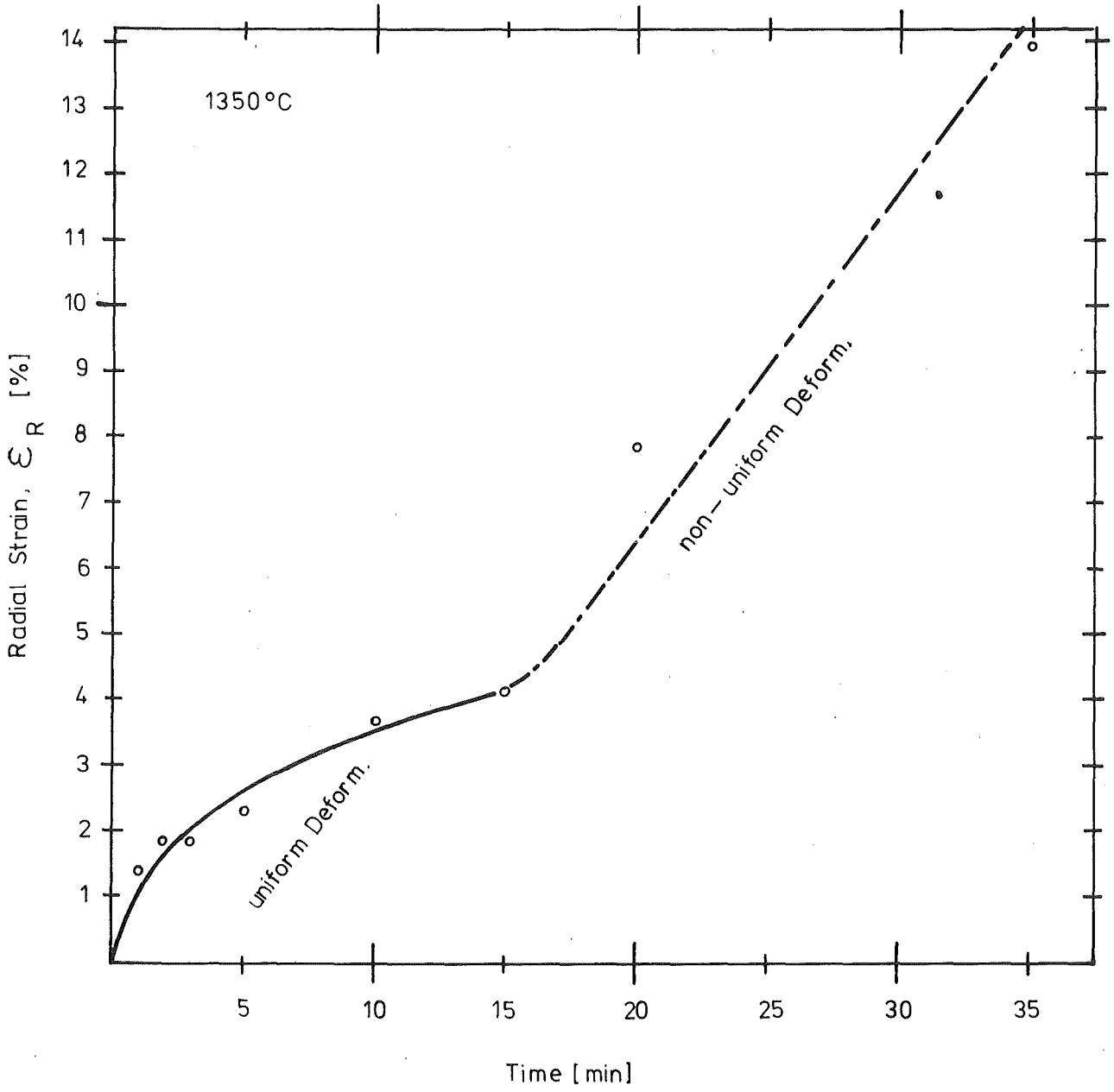

Fig. 5. Radial Strain of Zry-4 Tubing Induced by Oxidation at 1350° C

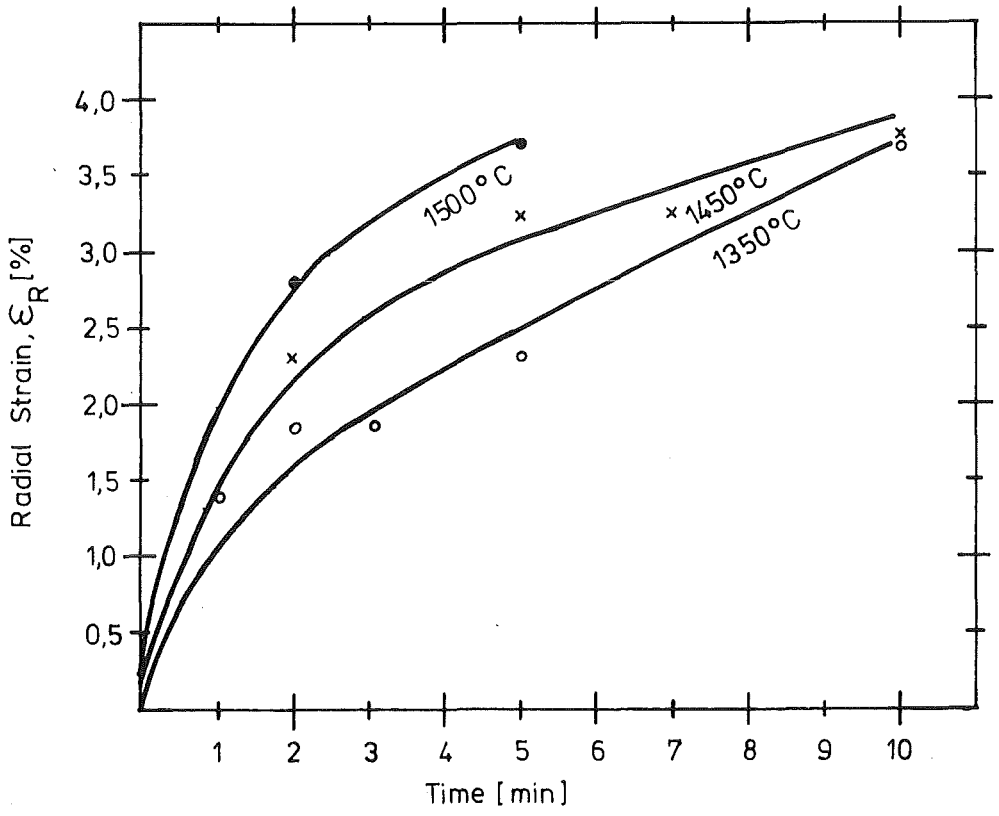

Fig.6 Oxidation-Induced Radial Strain at Different Temperatures

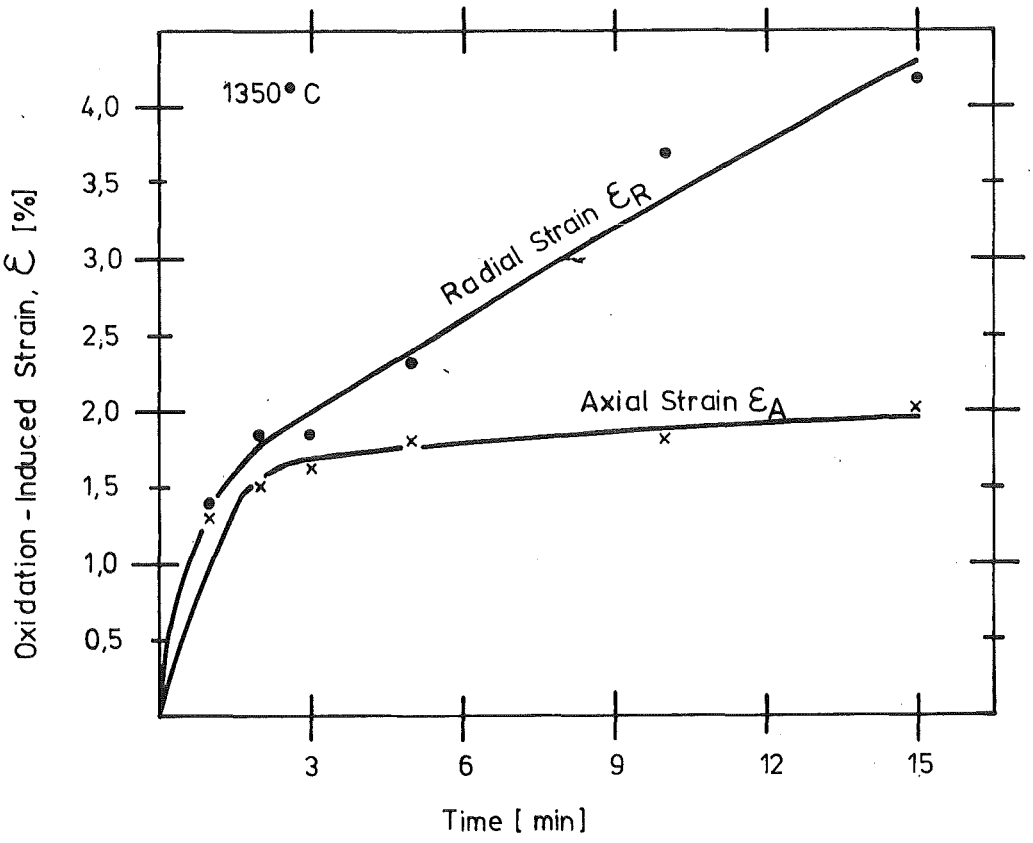

Fig.7. Oxidation Induced Radial and Axial Strain at 1350° C.

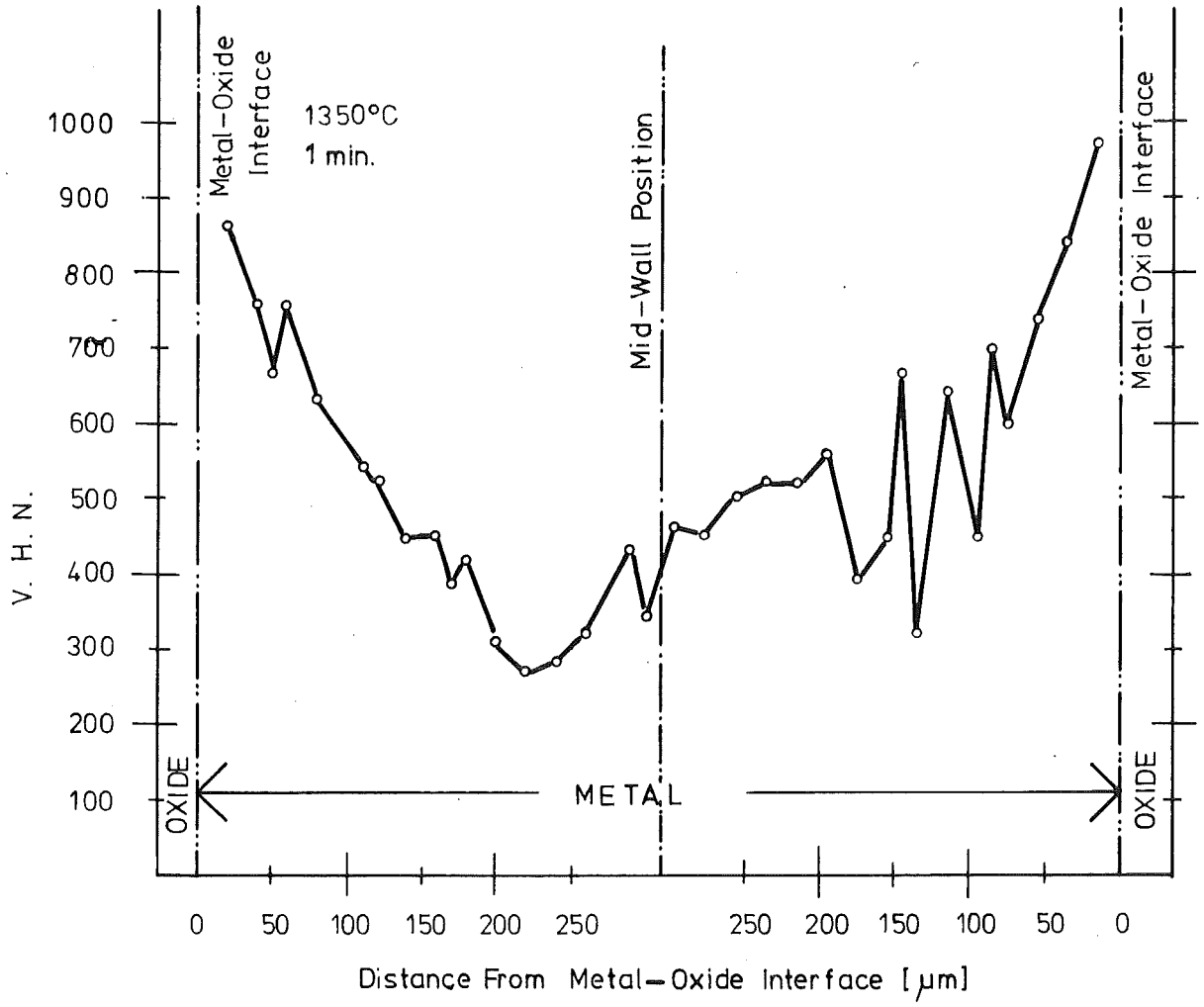

Fig. 8 Variation Of Microhardness With Distance From Metal-Oxide Interface.

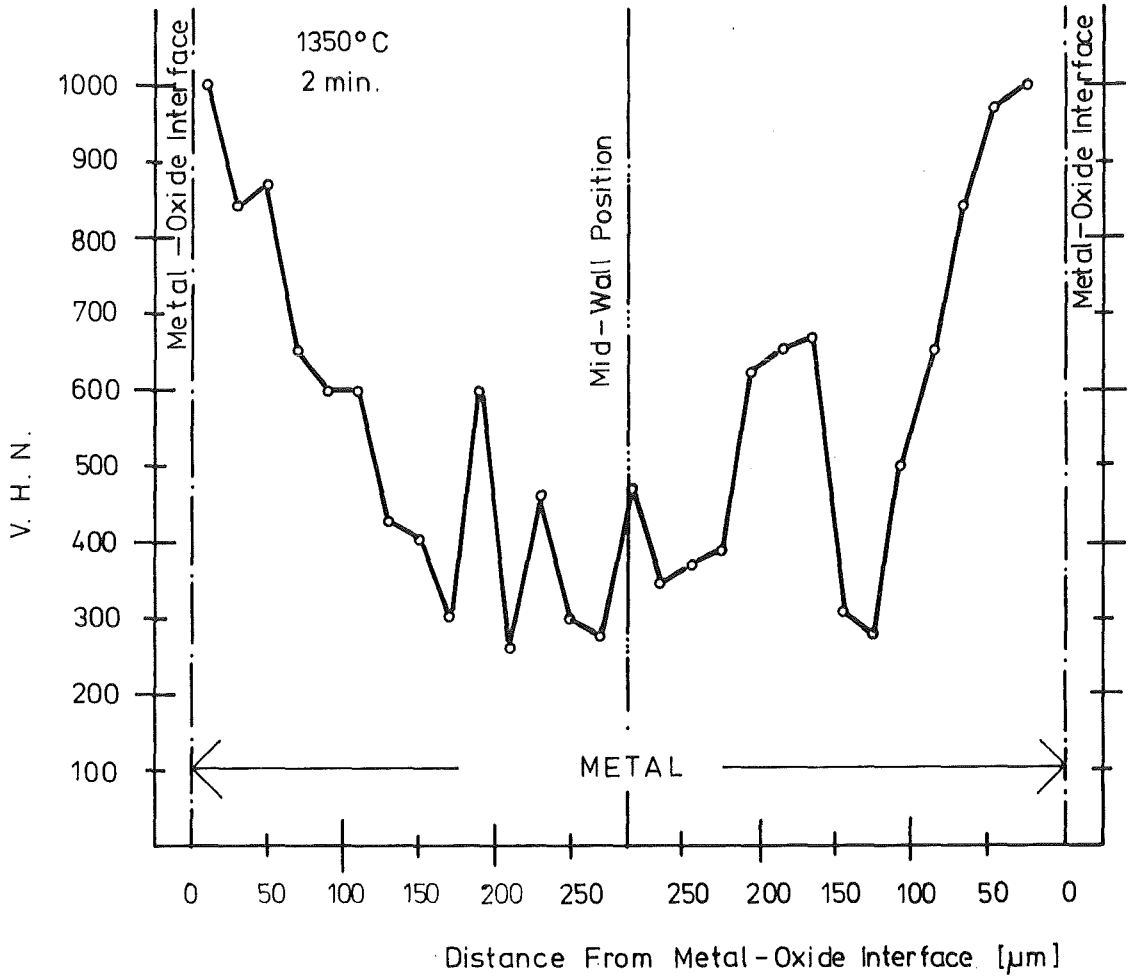

Fig. 9. Variation Of Microhardness With Distance From Metal- Oxide Interface.

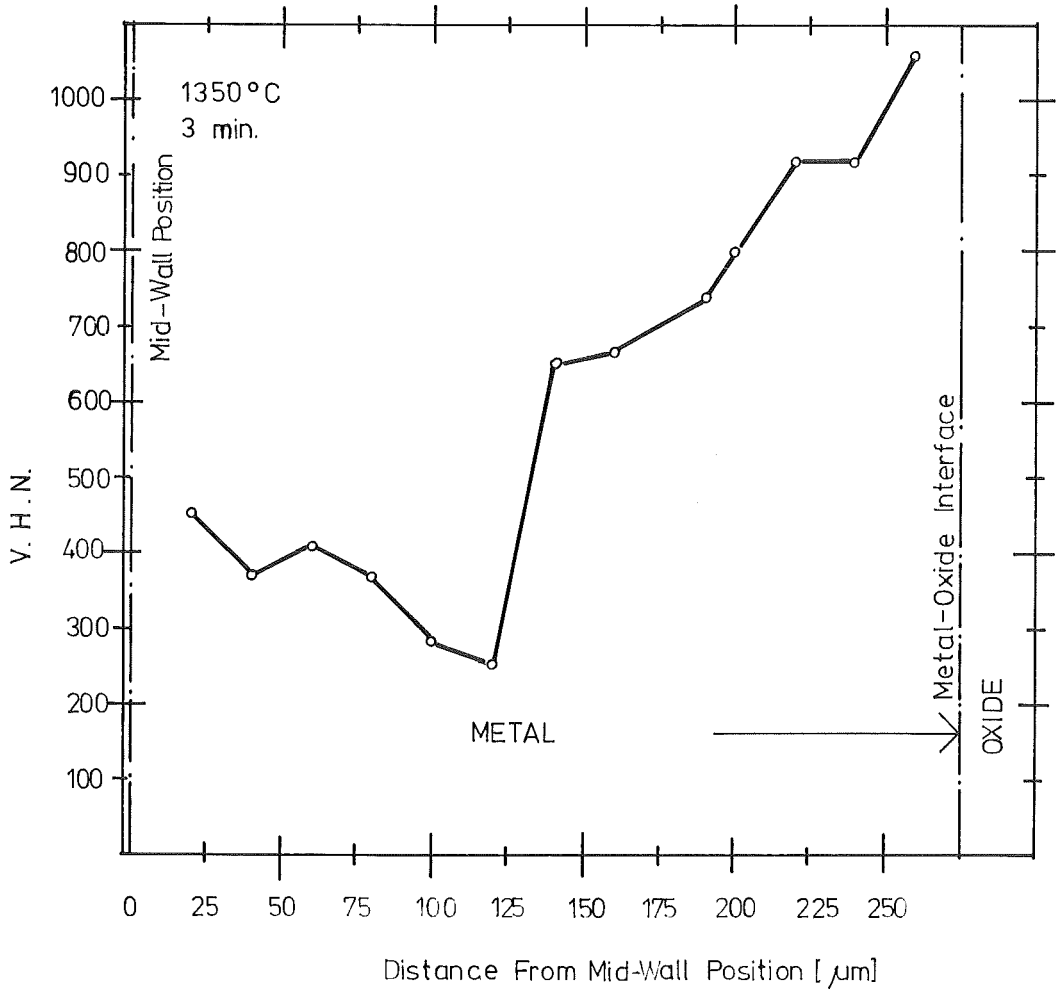

Fig.10. Variation Of Microhardness With Distance From Metal-Oxide Interface

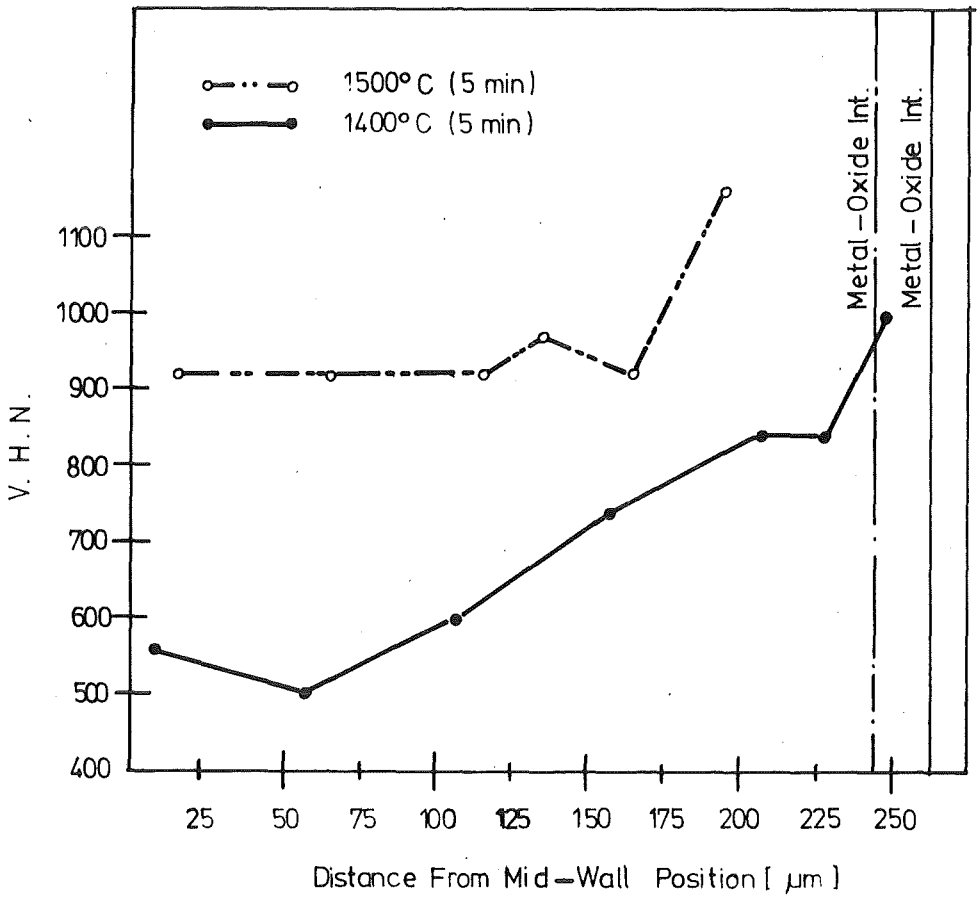

Fig. 11. Variation Of Microhardness With Oxidation Temperature

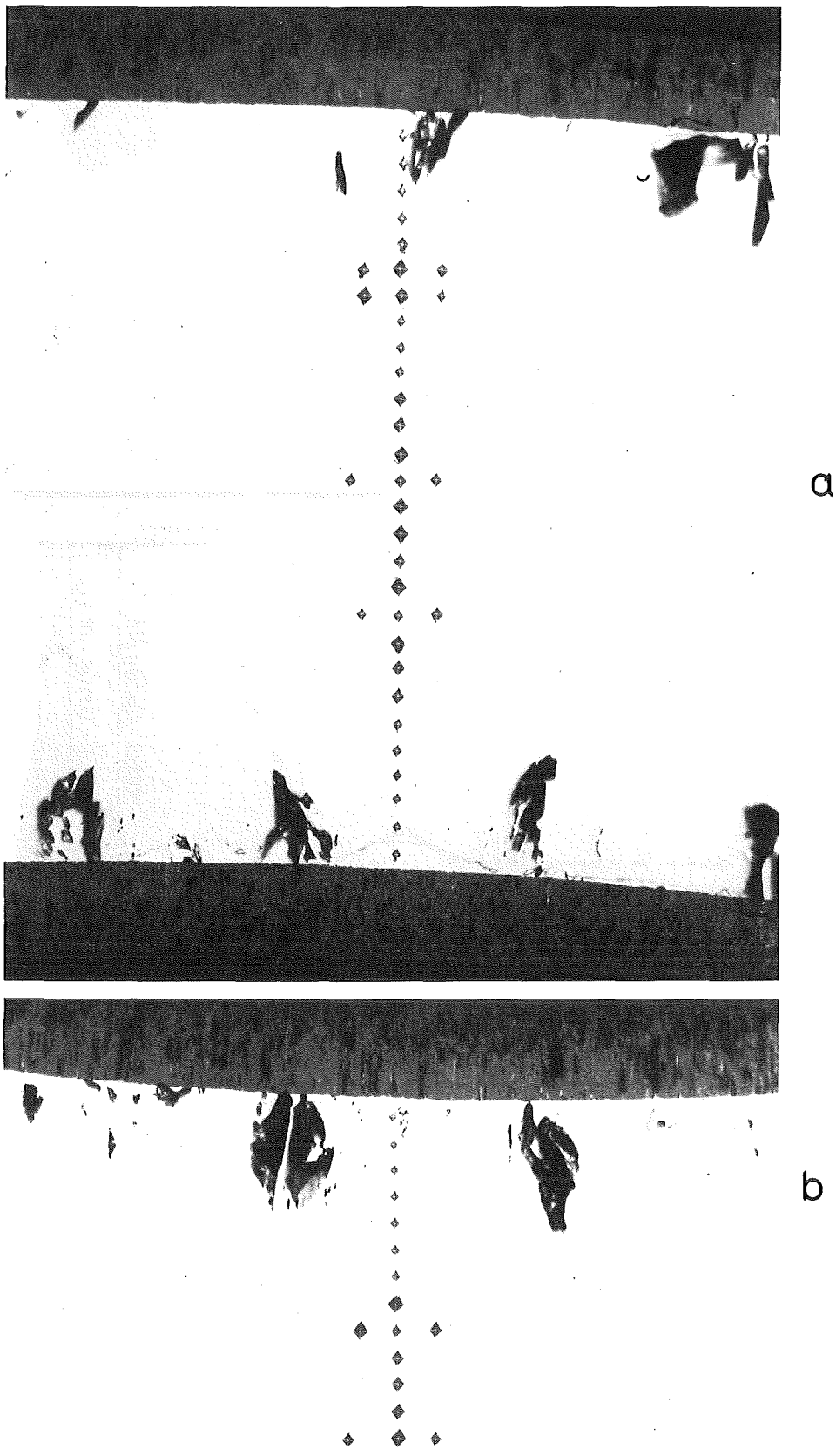

Fig.12. Microhardness Gradient Trough The Underlying Metal Of Zry-4 Tubing Oxidized At 1350°C, (a) 2min. And (b) 3min. (X 200)

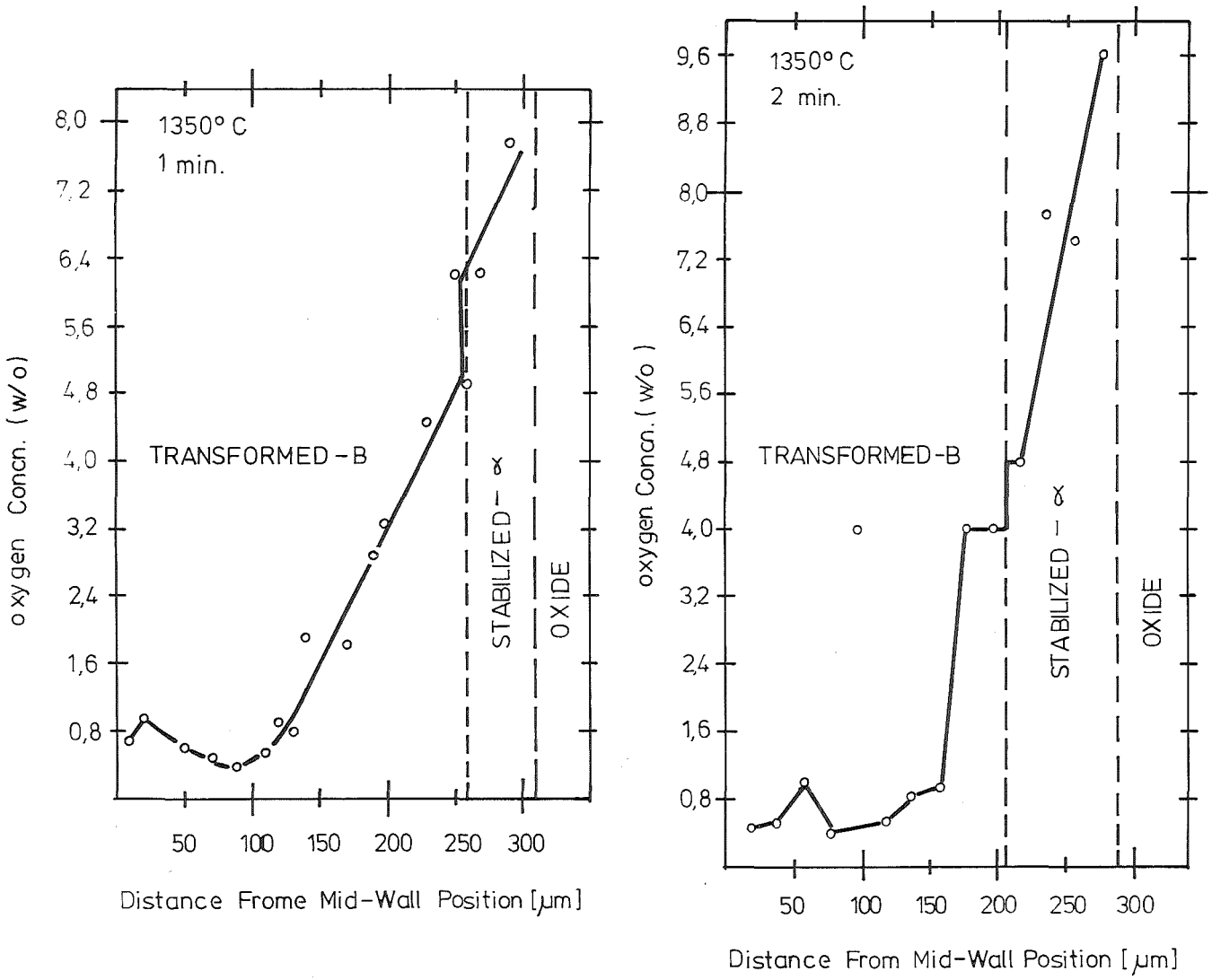

Fig.13. Variation Of Oxygen Concentration With Distance From Mid-Wall Position

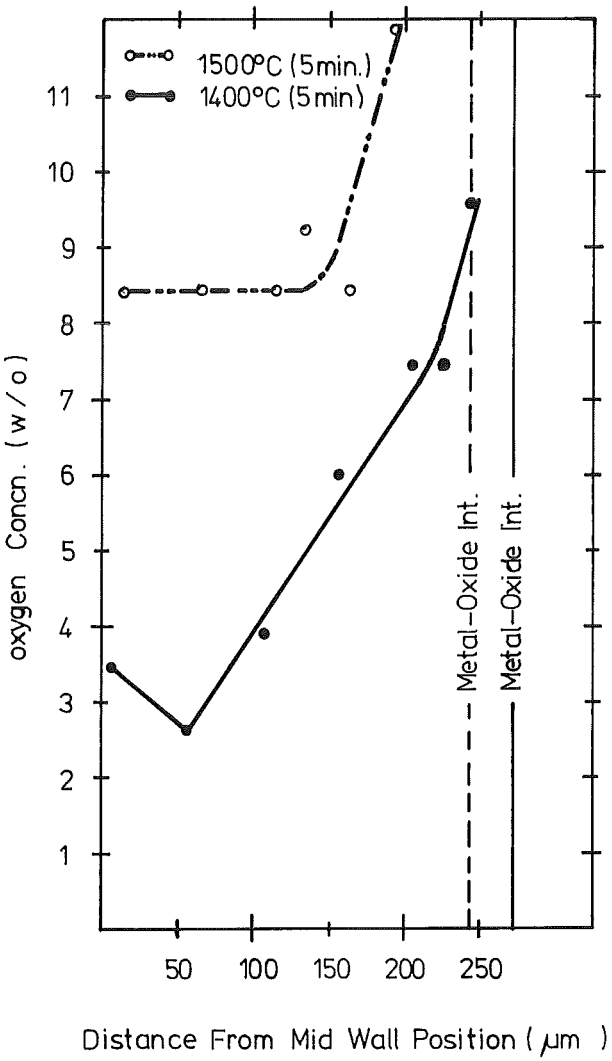

Fig.14. Variation Of Oxygen Concentration With Temperature

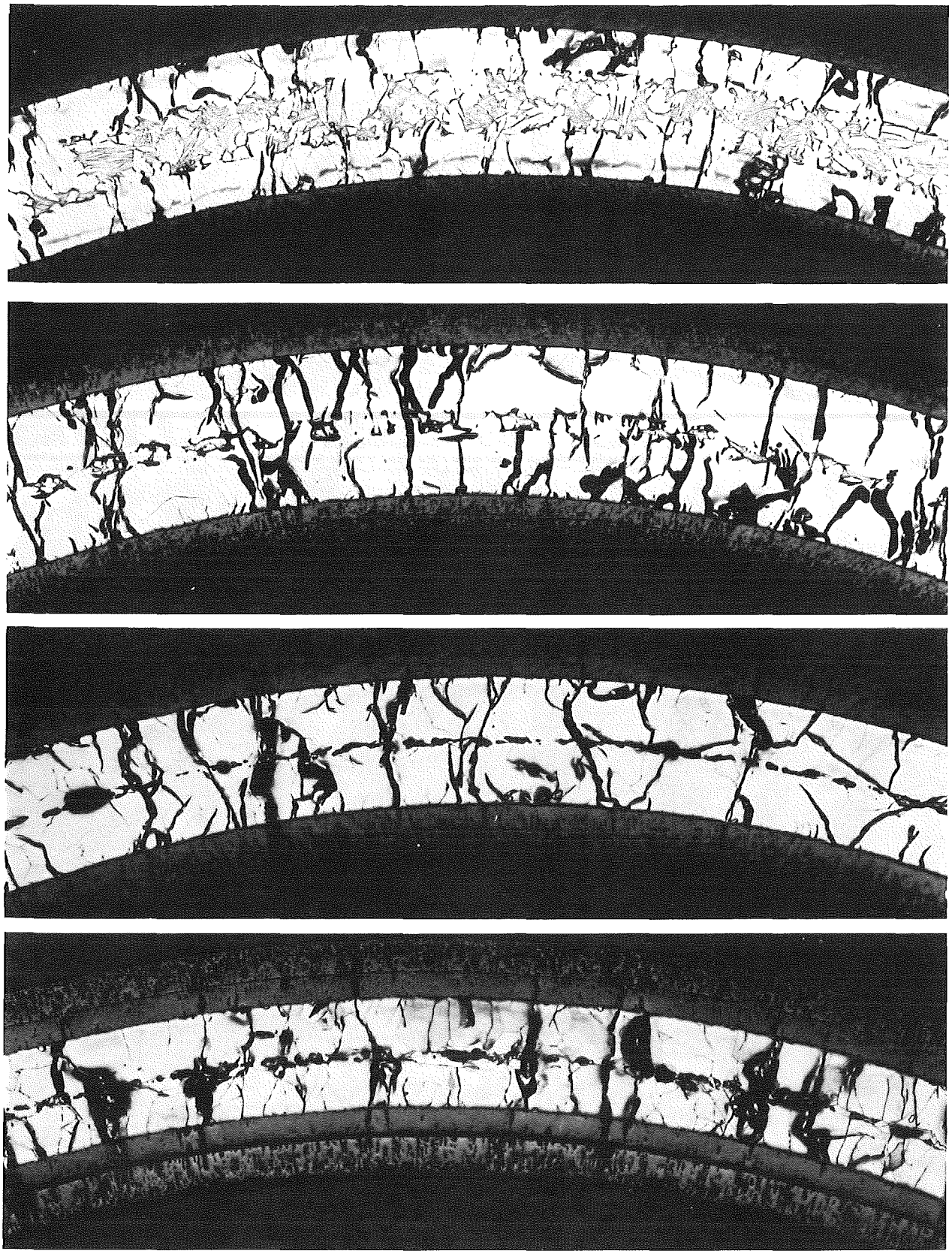

Fig.15. Zry-4 Tubing Oxidized At 1350°C For (a) 5 min. (b) 10 min. (c) 15 min. And (d) 25 min. (X 50)

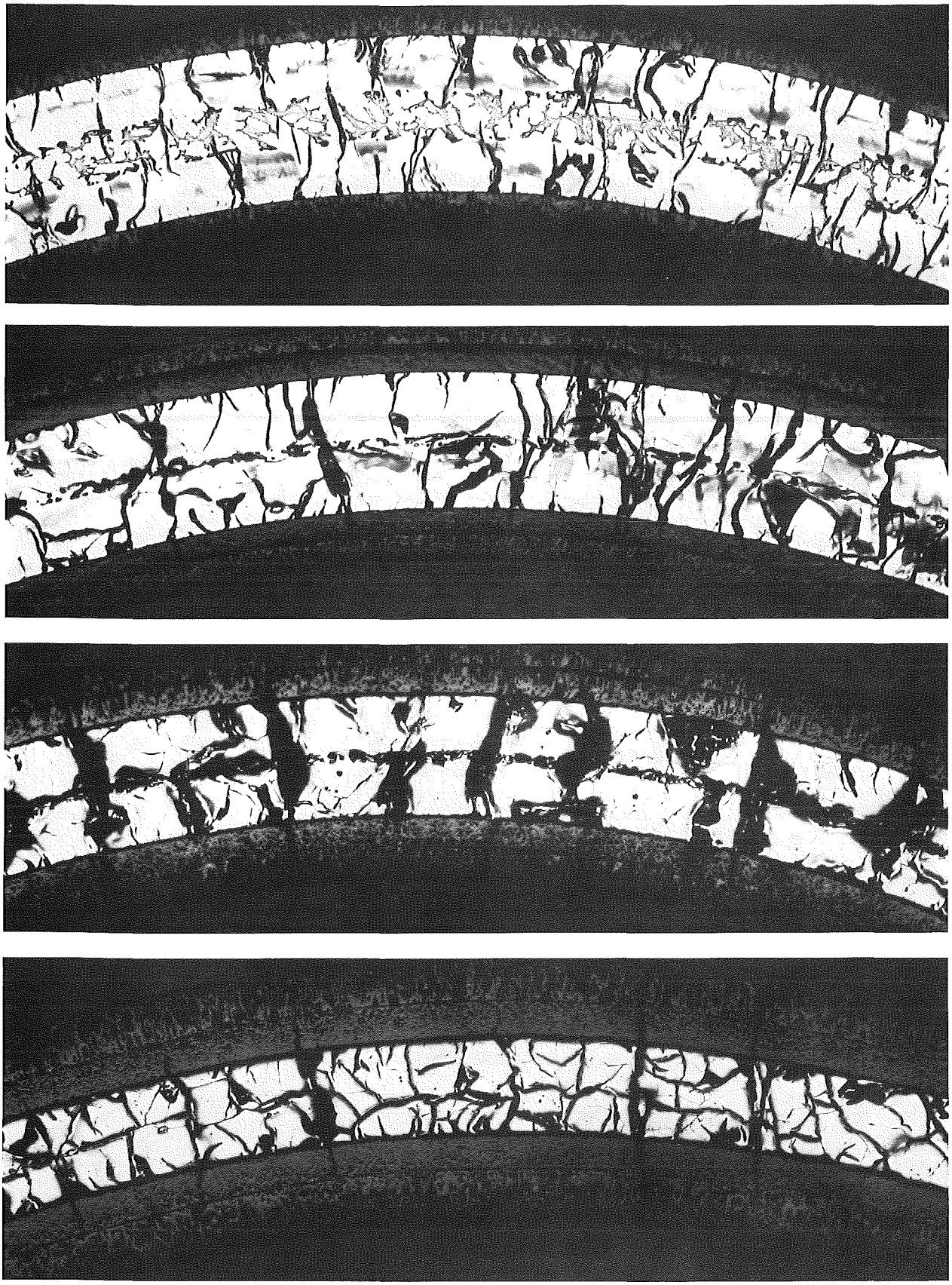

Fig.16. Zry-4 Tubing Oxidized At 1400°C For (a) 5 min. (b) 10 min. (c) 15 min. And (d) 25 min. (X 50)

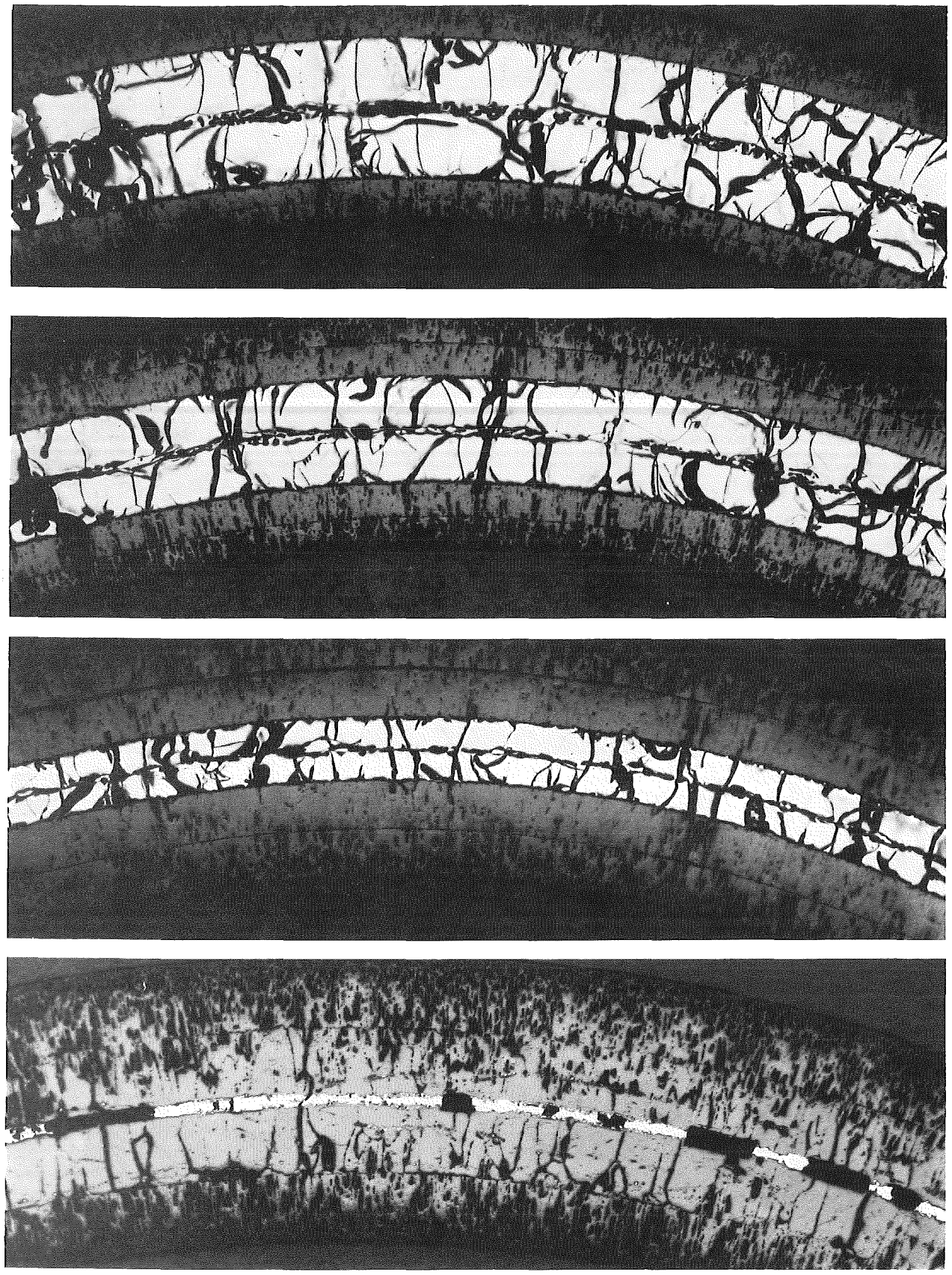

Fig.17. Zry-4 Tubing Oxidized At 1500°C For (a) 5 min. (b) 10 min. (c) 15 min. And (d) 35 min. (X 50)

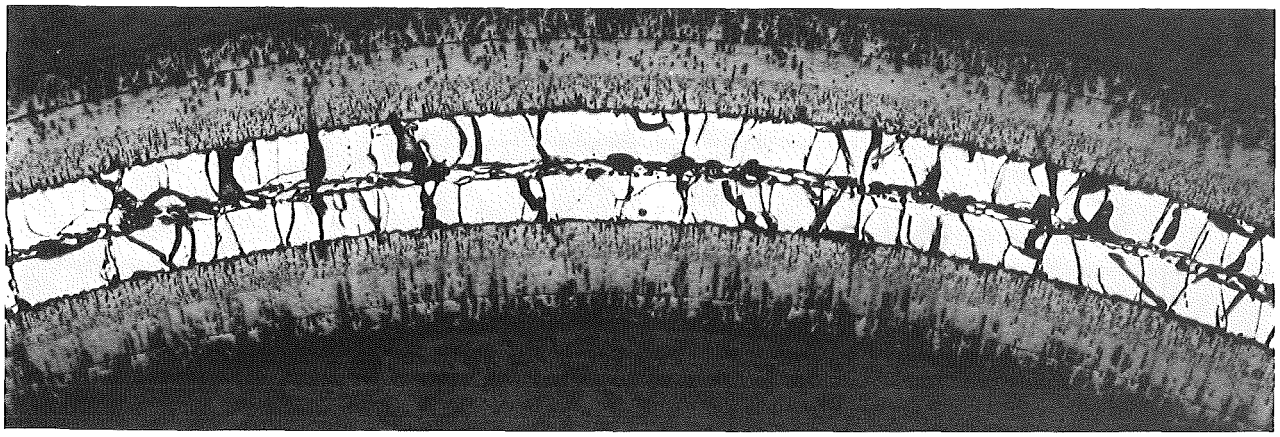

a

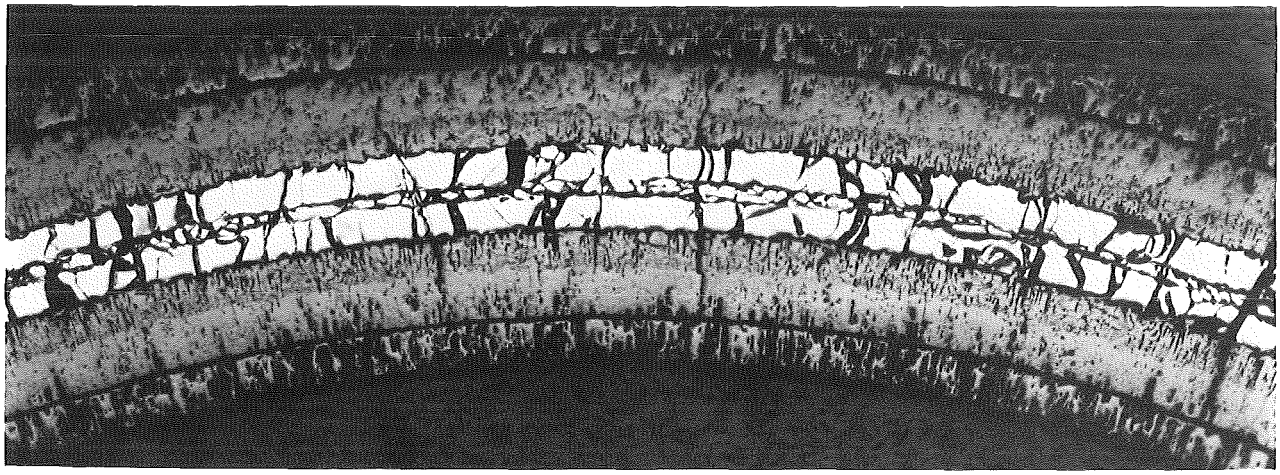

b

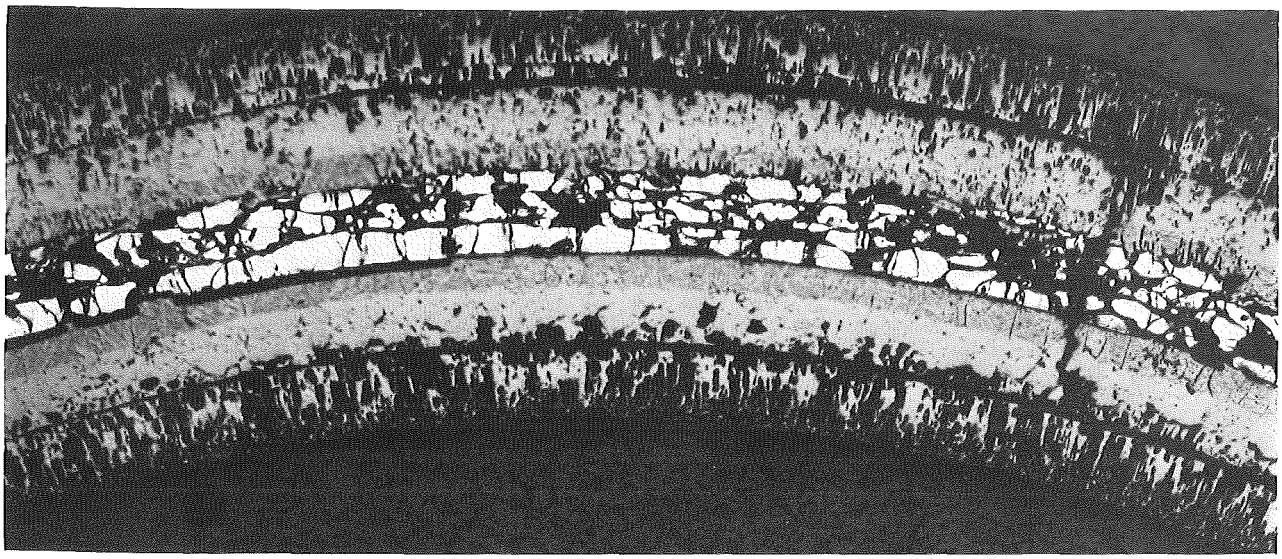

c

Fig.18. Zry-4 Tubing Oxidized At 1550°C For (a) 5min. (b) 10 min. And (c) 15 min. (X50)

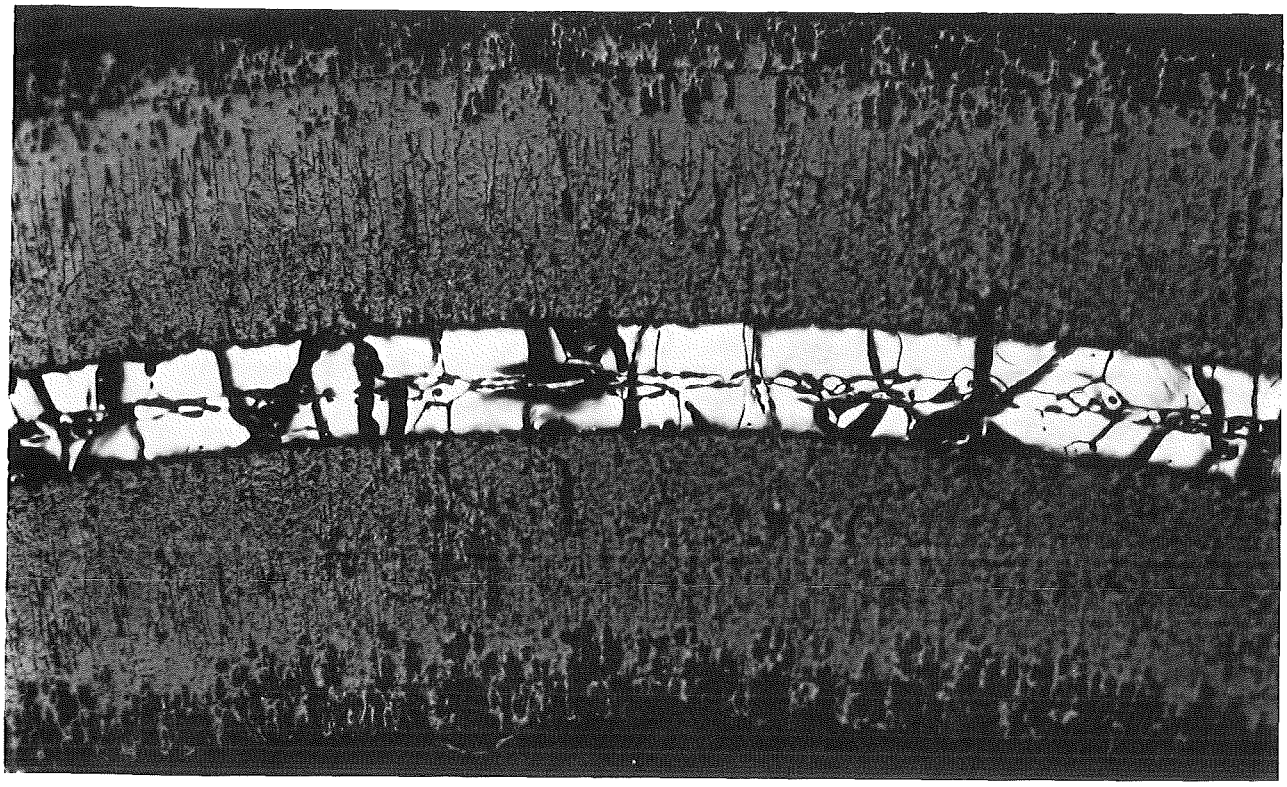

a

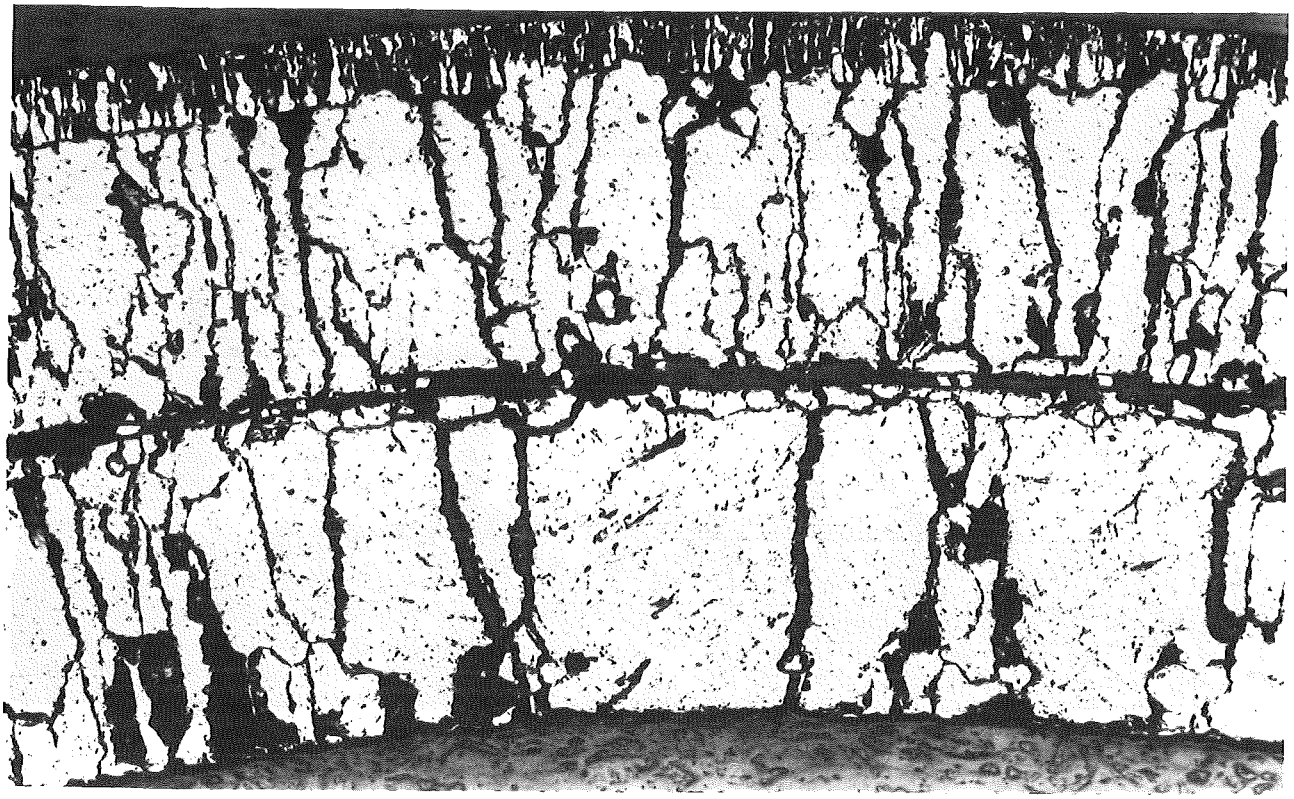

b

Fig.19. Zry-4 Tubing Oxidized At 1600°C For (a) 3 min. And (b) 5 min. (X 100)

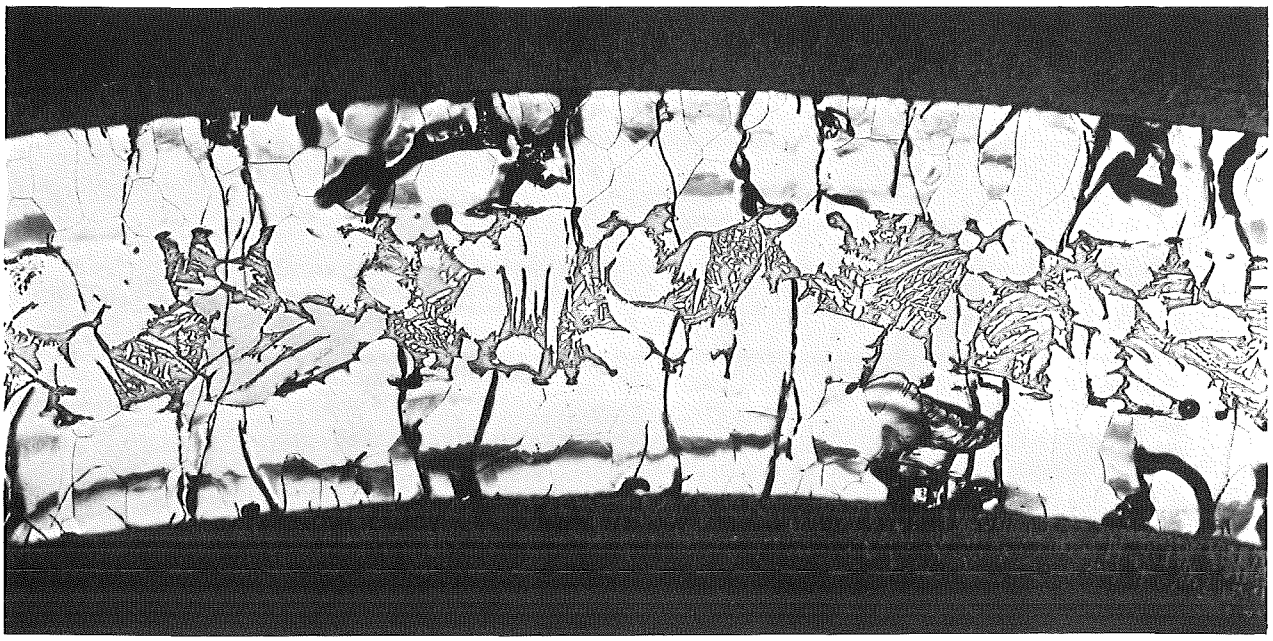

a

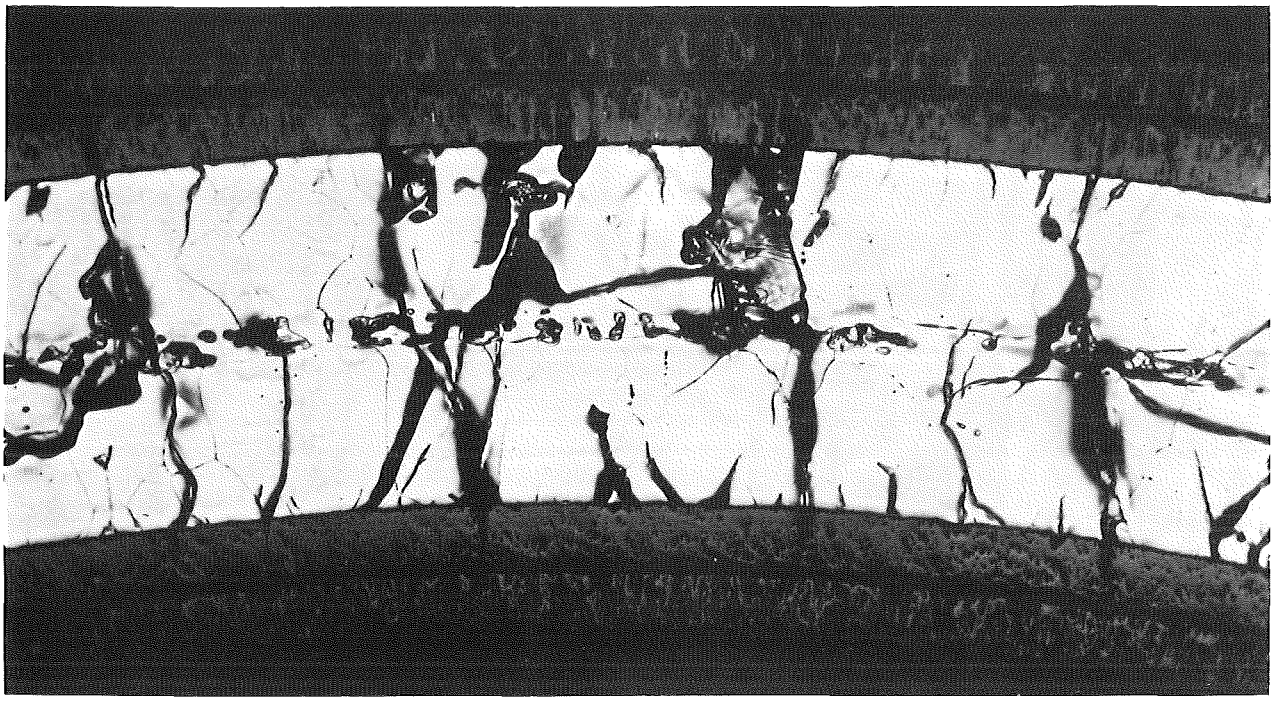

b

KfK

Fig. 20. Zry-4 Tubing Oxidized At (a) 1350°C - 5 min. And (b) 1400° C - 10 min. (X 100)

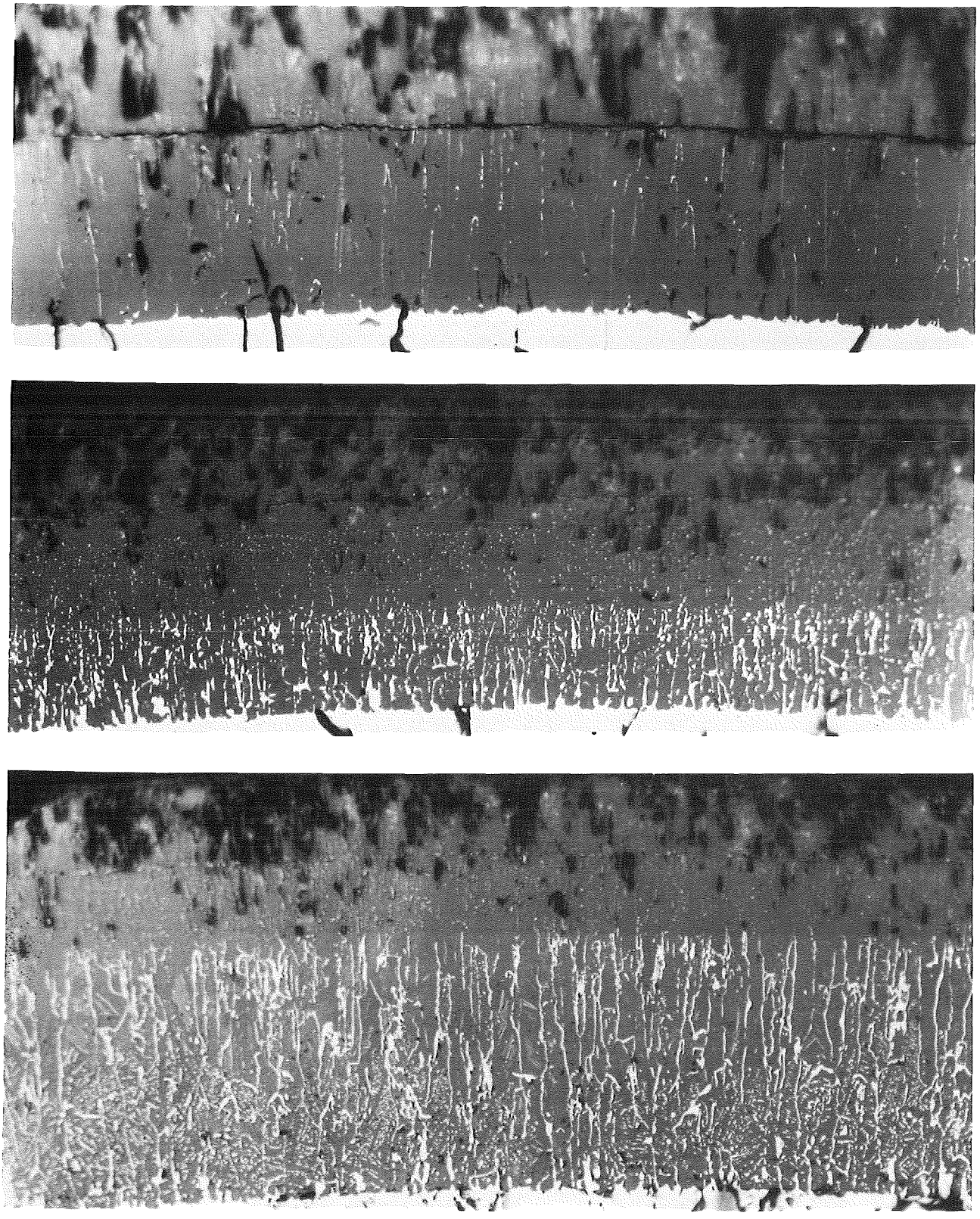

Fig. 21. Zry – 4 Tubing Oxidized At (a) 1500°C–15 min., (b) 1550°C– 5 min. And (c) 1600°C–3 min. (X 200)

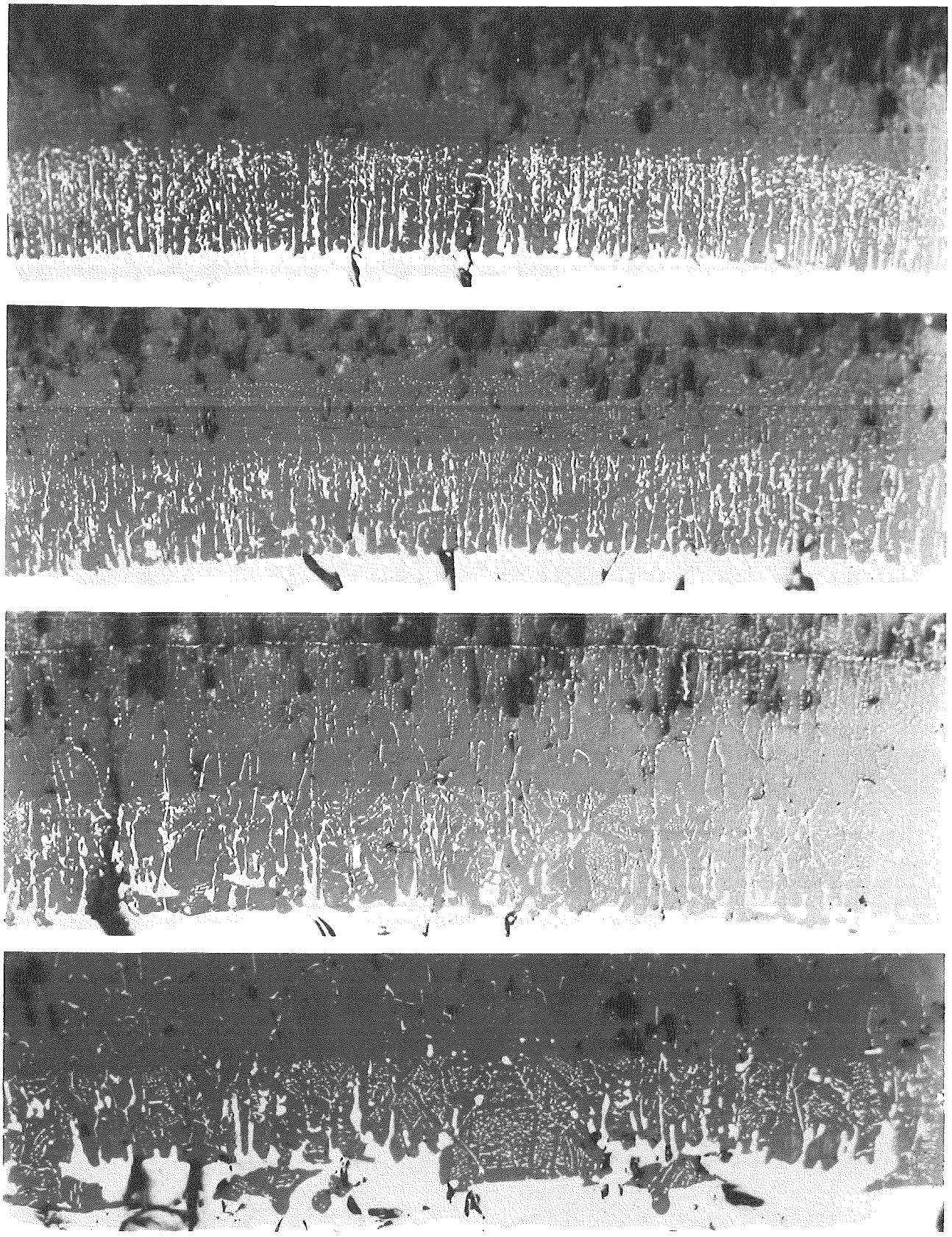

Fig. 22. Zry-4 Tubing Oxidized At 1550°C For (a) 2 min., (b) 5 min., (c) 10 min. And (d) 15 min. (X 200)

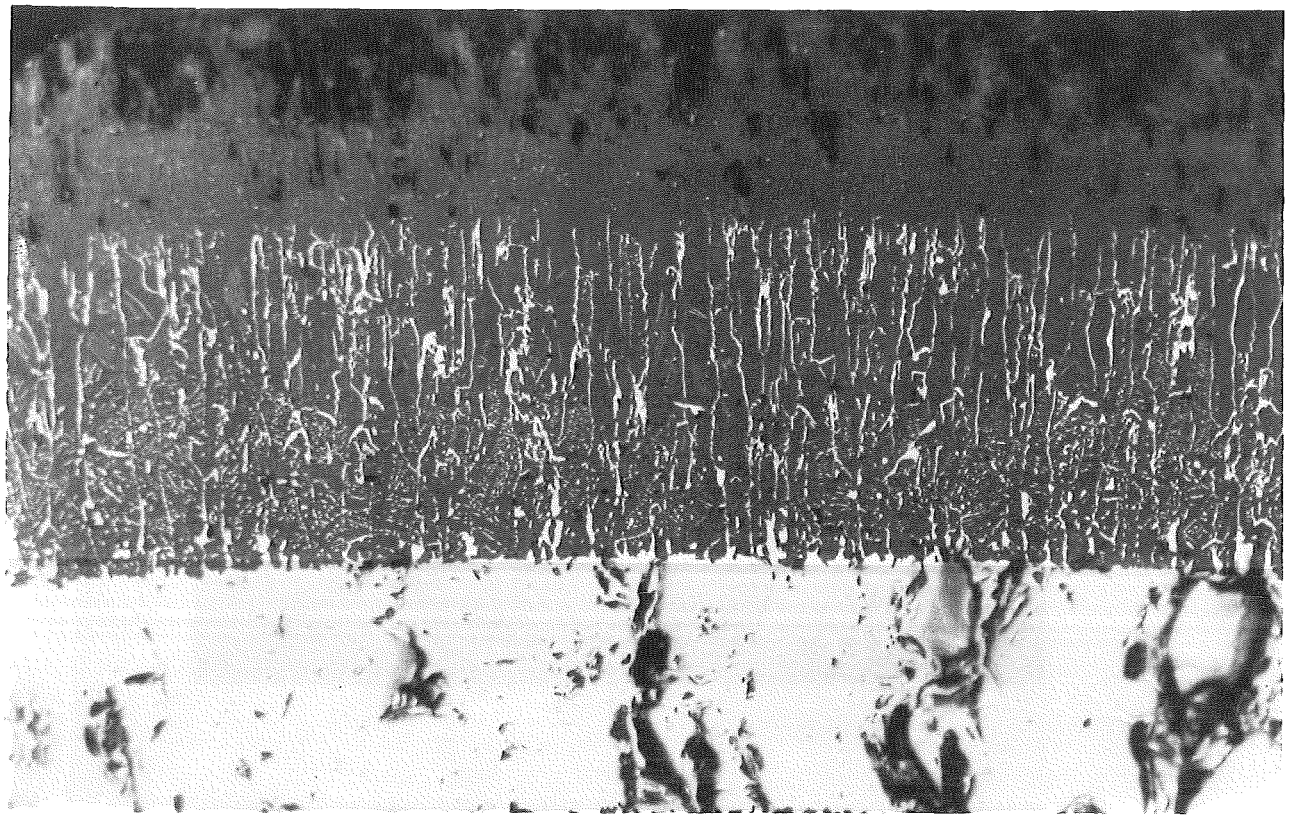

a

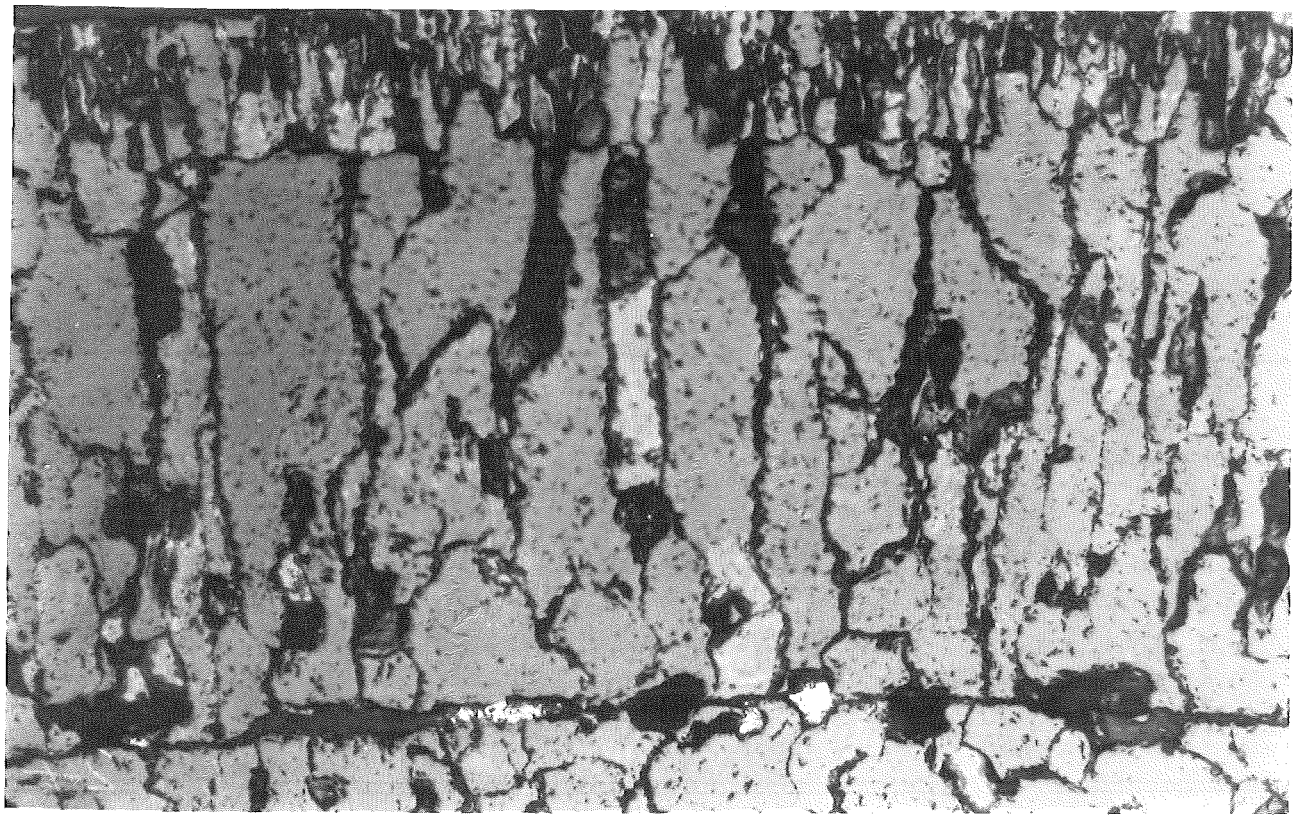

b

KfK

Fig. 23. Zry-4 Tubing Oxidized At 1600°C For (a) 3 min. And (b) 5 min. (X200)

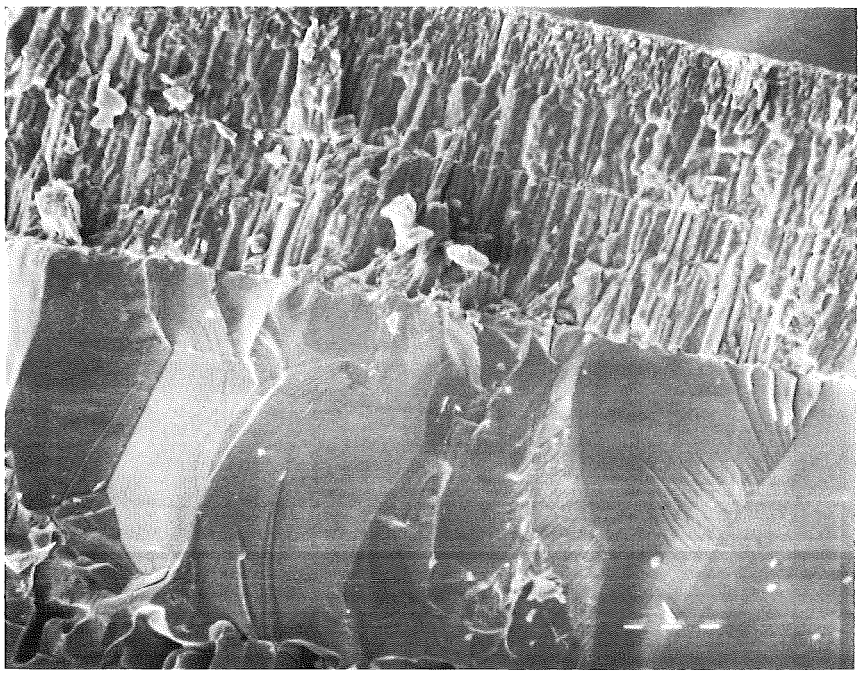

a

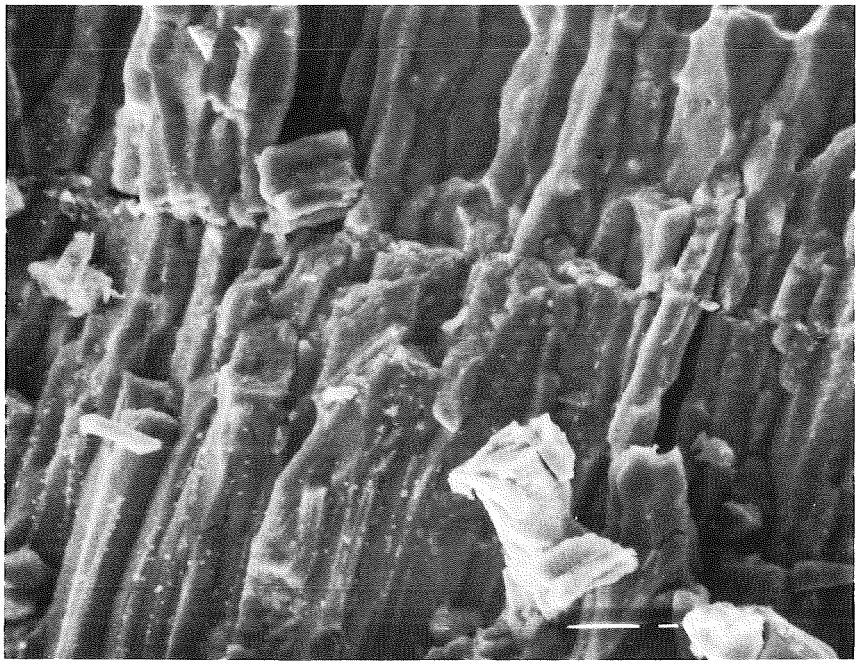

b

Fig. 24. SEM Fractographs Of Zry-4 Tubing Oxidized At 1500 °C For 5 min. (a) X 300 And (b) X 1000

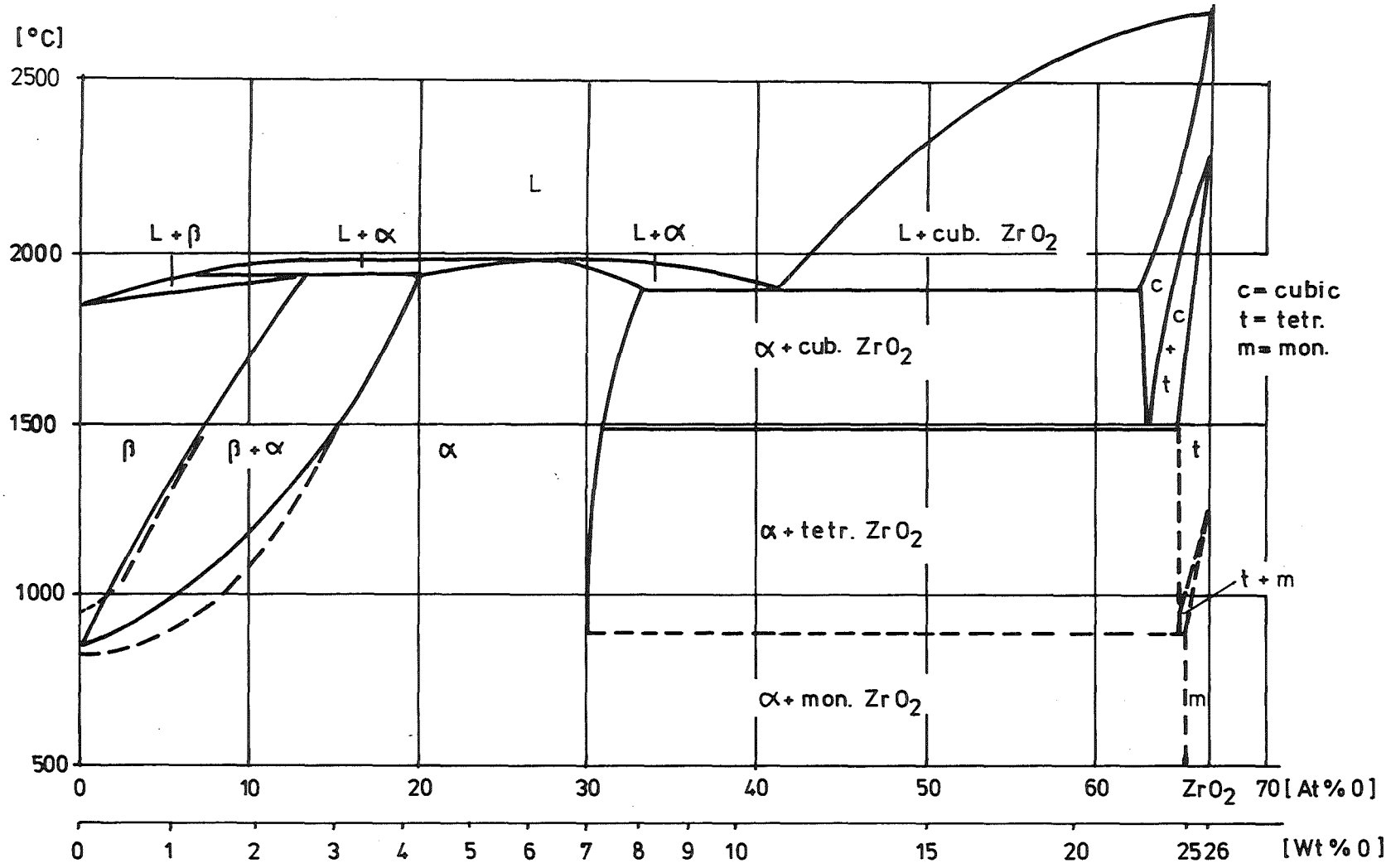

Fig. 25 Zirconium – Oxygen System (From ref. 24)